University of Michigan
College of Literature, Science, and the Arts
Department of Molecular, Cellular, and Developmental Biology

Myosin Binding Protein C Mutation Locus and Type Affect Hypertrophic Cardiomyopathy Disease Mechanism

Neha Hafeez

A senior honors thesis submitted in partial fulfillment of requirements for the Degree of Bachelor of Science in Cellular and Molecular Biology with Honors
- December 2017 -

Table of Contents

Abstract

Hypertrophic cardiomyopathy (HCM) is a cardiovascular disease characterized by thickening of the left ventricular wall presented with increased interstitial fibrosis and structural disarray.[1] HCM is typically caused by mutations in genes encoding for sarcomere proteins; ~50% of these mutations are found in cardiac Myosin Binding Protein C (MYBPC3).[2] We aim to better understand disease pathogenesis of human MYBPC3 mutations through murine and primary cardiomyocyte models.

Mutant mouse transgenic models do not develop the HCM disease phenotype, likely due to intrinsic cardiac and hemodynamic differences between mice and humans or inadequate mutant protein expression in the mice.[3] Therefore, I switched to characterizing these mutations using human MYBPC3 constructs that express in neonatal rat ventricular cardiomyocytes (NRVMs) via adenoviral transduction. We characterize several human MYBPC3 truncating mutations along the length of the gene and non-truncating mutations clustered at the C3, C6, and C10 domains by analyzing protein localization, expression, stability, and interaction with molecular chaperone proteins. We find that truncating and non-truncating MYBPC3 mutants causes disease via protein dosage effects and altered function, challenging the idea that truncating mutants are solely loss-of-function and non-truncating mutants are solely gain-of-function. Specifically, we find that non-truncating mutations in the C10 domain may lead to loss-of-function due to reduced protein dosage and aberrant localization. We also show that knockdown of the molecular chaperone, Hsc70, results in decreased MYBPC3 degradation rates and Hsc70 activation results in increased MYBPC3 degradation rates, indicating that Hsc70 interacts with MYBPC3 to facilitate protein degradation. Differences in degradation rates indicate differences in protein stability among the mutants, potentially due to altered interaction with molecular chaperones. These findings provide new insights into different categories of MYBPC3 mutations and their role in the HCM phenotype, which could be used in the future to identify ideal therapies for HCM patients based on their specific mutation.

Introduction

Hypertrophic Cardiomyopathy

Hypertrophic Cardiomyopathy (HCM) is an inherited cardiovascular disease displaying dominant Mendelian inheritance with a prevalence of up to one in 500 people in the general population.[4] HCM has been found in populations around the world, affecting people of various ethnic backgrounds and both sexes.[5] Symptoms of hypertrophic cardiomyopathy range from mild cases of lightheadedness, heart palpitations, and syncope to more severe cases of stroke, sudden cardiac death, heart failure, and atrial fibrillation. This variability in disease penetration among individuals makes it difficult to predict disease severity.[6,7]

Hypertrophic cardiomyopathy is characterized by thickening of the left ventricular wall (Figure i) that occurs without increased external load[1]. Affected individuals have enlarged cardiomyocytes, increased interstitial fibrosis and myocardial disarray.[2] This morphology impairs cardiac relaxation, increasing the likelihood of heart failure.[8] It is diagnosed primarily via echocardiography and cardiac magnetic resonance imaging (MRI).[9] Such imaging techniques allow for a physician to identify left ventricular hypertrophy, myocardial fibrosis, and impaired diastolic function during resting and exercise states. Examining heart function under exercise stress allows for physicians to better understand HCM symptoms arising during physical exertion.[9] Patients can then undergo targeted genetic testing to determine the genetic basis behind their symptoms and inform family members who may be potential carriers.[10] Primary interventions for HCM patients often include septal myectomy to correct outflow tract obstruction and implantable cardioverter defibrillators to protect against arrhythmias.[11]

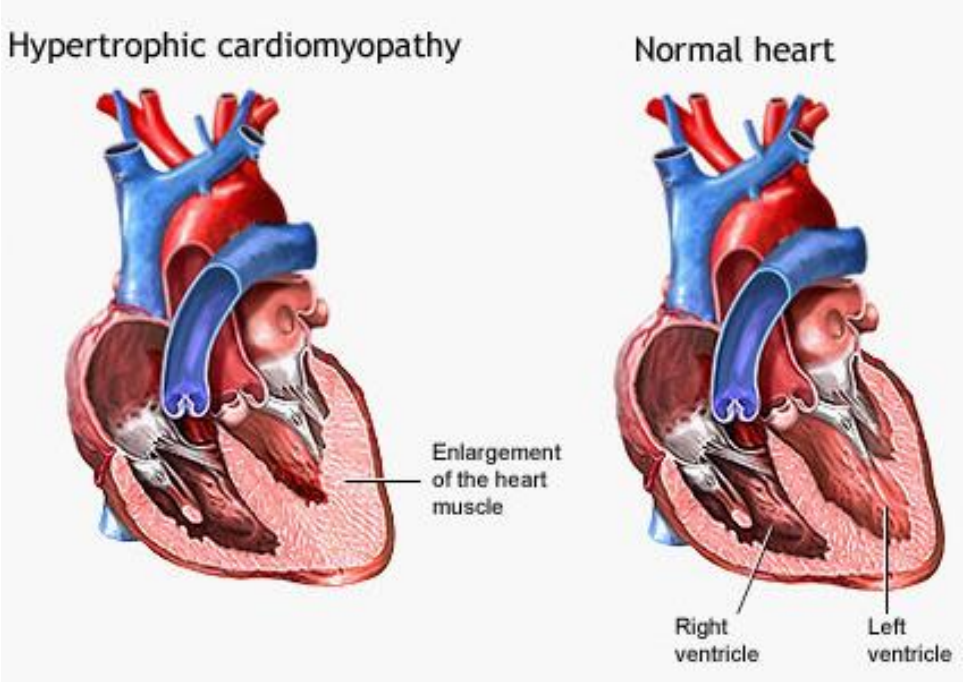

Figure i: Hypertrophic ventricular remodeling in HCM. The left ventricle wall and intraventricular septum are thicker in the HCM heart. Figure adapted from the Minneapolis Heart Institute Foundation.

HCM is caused primarily by mutations in genes encoding the thick and thin contractile myofilament protein components of the sarcomere or the adjacent Z-disc.[2] Over 1500 such mutations are currently known, the majority of which are in cardiac Myosin Binding Protein C (*MYBPC3*) and the cardiac β-myosin heavy chain (*MYH7*) genes (Figure ii).[4] More than 90% of HCM mutations are inherited as an autosomal dominant disease, which means that offspring of affected individuals have a 50% probability of inheriting the mutation.[8] Such inheritance patterns have resulted in the prevalence of founder mutations in smaller, more homogenous populations.[12] For example, the *MYBPC3* c.2373_2374insG mutation was detected in almost 25% of all HCM patients in the Netherlands.

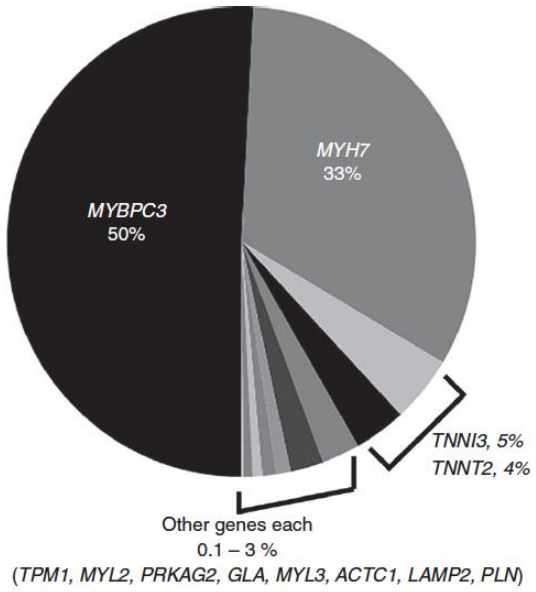

Figure ii: Genes containing mutations resulting in HCM. Genes and their estimated frequency for HCM causing mutations. Figure adapted from Alfares *et al.*, 2015

Cardiac Myosin Binding Protein C

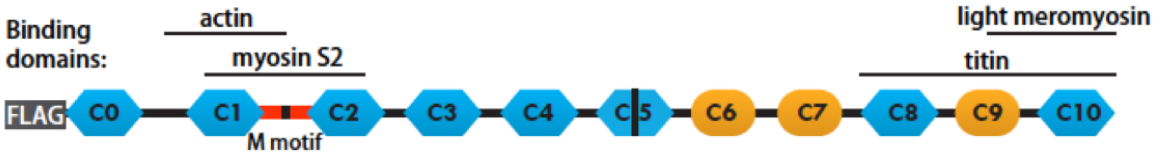

Figure iii: Cardiac Myosin Binding Protein C Domains Diagram cMyBPC is composed of eight Immunoglobin-like domains (blue hexagons) and three fibronectin-3-like domains (orange ovals). MYBPC3 binds to actin and myosin S2 via domains near its N-terminus (C1-C2) and binds to light meromyosin and titin via its C-terminal domain C10. Figure adapted from Amelia Glazier, Sharlene Day Lab.

Cardiac Myosin Binding Protein C is a 150kDa sarcomeric protein that is involved in thick filament structure and contractility regulation (Figure iv).[13] It binds to light meromyosin and titin near its C-terminal domain, anchoring the protein to the thick filament backbone in the sarcomere.[14] This interaction has been shown to have structural and mechanical roles in proper muscle

contraction.[15] Additionally, phosphorylation sites within the M-domain mediate electrostatic binding with myosin S2 and actin, affecting cross-bridge cycling.[16,17]

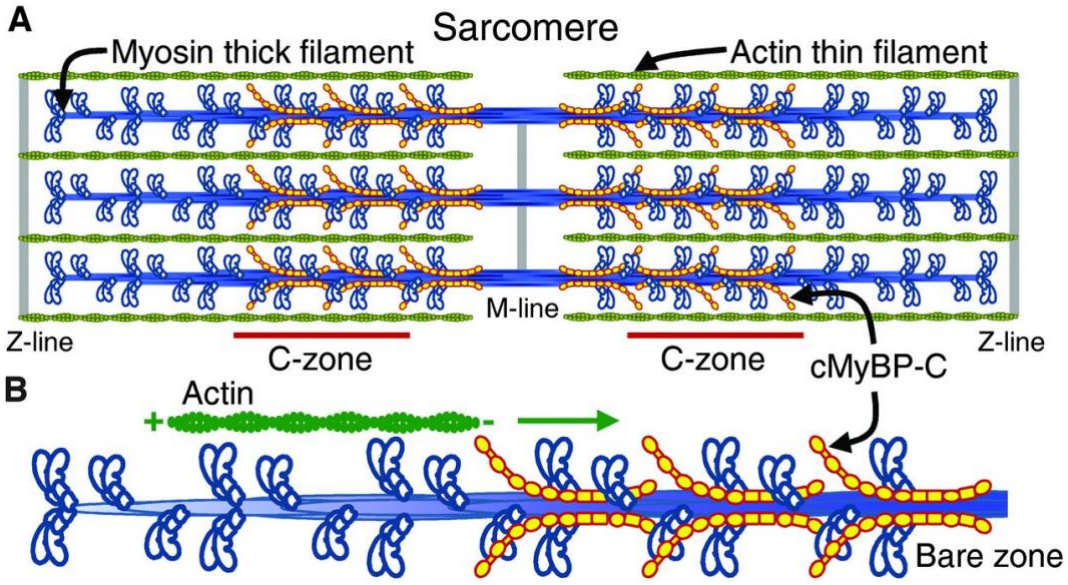

Figure iv: Sarcomere thick filaments and MYBPC3. Cardiac Myosin Binding Protein C localizes to the myosin thick filament C-zones. Figure adapted from Previs *et al.*, 2012.

MYBPC3 mutations have been associated with a wide range of severity in the HCM phenotype.[18] Previous studies have also shown that about 90% of MYBPC3 mutations result in premature termination codons and are typically associated with a more severe HCM phenotype than those resulting from missense or in-frame deletions.[2] However, the missense mutation, Arg502Trp, is the single most common mutation in HCM patients with prevalence estimates of 2.4% among Caucasian patients with HCM.[19] Therefore, we aim to better understand the mechanism by which mutation type affects the disease phenotype. Interestingly, analysis of HCM patient registries, such as the Sarcomeric Human Cardiomyopathy Registry (SHaRe) indicate the presence of truncating mutations throughout the entirety of the MYBPC3 gene; however, non-truncating mutations appear to cluster in the C3, C6, and C10 domains (unpublished analysis, Sharlene Day, MD). Therefore, I also examine the effect of mutation locus in the context of the disease mechanism in this study.

There are currently two prevailing hypotheses for MYBPC mutations in disease pathogenesis: haploinsufficiency and the "poison peptide" hypotheses.[20] The haploinsufficiency hypothesis stipulates that the phenotype is due to insufficient protein levels within the sarcomere, whereas poison peptide hypothesis states that the mutant proteins act as dominant negative proteins and incorporate into the sarcomere myofilament.[21] Previously established models propose that these hypotheses are mutually exclusive, where the truncating mutants act solely via a loss-of-function mechanism and non-truncating mutants act solely via a gain-of-function mechanism. However, in this paper, I challenge these models and hypothesize that the mutations contribute to the disease phenotype via a combined effect of protein dosage and altered function.

Proteostasis and Chaperone Protein Interactions

Protein homeostasis, or proteostasis, is crucial for health of the proteome, and the cell overall.[22] The stability and function of each protein within the proteome is dependent on the interactions of the proteostasis network, which includes but is not limited to molecular chaperone activity, the ubiquitin-dependent proteasome, and autophagic processes.[23] Regulation of the proteostasis network is orchestrated by pathways including the heat-shock response (HSR), oxidative stress response (OSR), and the unfolded protein response (UPR).[22] HSR regulates the expression of various molecular chaperones, OSR regulates cell stress due to overabundance of reactive oxygen species, and UPR acts to clear unfolded proteins that accumulate due to endoplasmic reticulum stress.[24] Dysfunction of these cellular stress response mechanisms can lead to various protein conformational diseases (Figure v, vi); for example, loss of function mutations in the protein co-chaperone, BCL-2-associated anthanogene 3 (BAG3), has been shown to disrupt proteostasis and cause cardiomyopathy.[25,26]

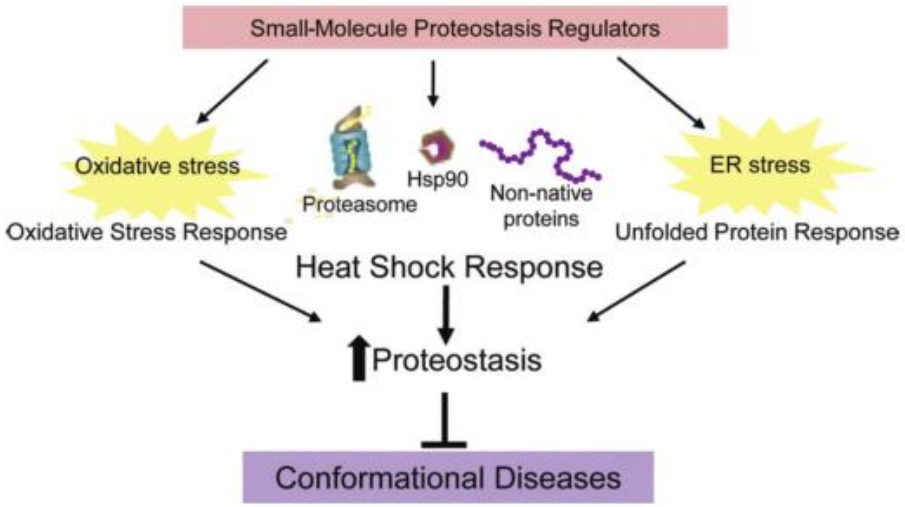

Figure v: Proteostasis and cellular stress response mechanisms. Diagram depicting various components of the proteostasis network. Figure adapted from Morimoto *et al.*, 2011

In this study, we are specifically looking at the heat shock response pathway within the context of MYBPC3 mutant proteins, specifically examining its interactions with the molecular chaperones of the Heat Shock Protein 70kDa (Hsp70) family. We hypothesize that the MYBPC mutants potentially have altered interactions with molecular chaperones, resulting in proteostatic dysfunction and contributing to the disease phenotype (Figure vi).

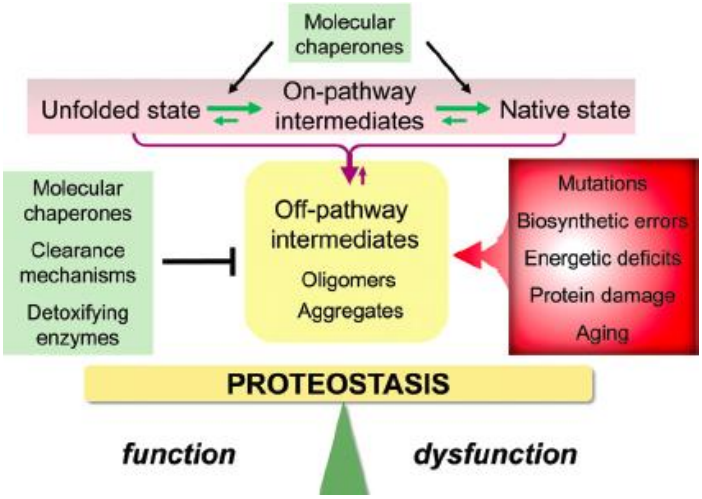

Figure vi: Molecular chaperones and proteostasis. Diagram depicting the role of molecular chaperones in proteostasis function. Figure adapted from Morimoto *et al.*, 2011.

Part 1: Animal Model of Hypertrophic Cardiomyopathy

Results

HCM phenotype not detectable in transgenic mouse model

To study the phenotype resulting from truncating MYBPC3 mutations, we began by characterizing the wild type and MYBPC3 mutant phenotype in mice. Nontransgenic and transgenic mice expressing a 75 kDa MYBPC3 truncating mutation in the C5 domain under the α-myosin heavy chain promoter on a background with two wild-type endogenous MYBPC3 alleles were assessed in mice ages ranging from 3 months to 12 months.[27] Ventricular tissue samples were then collected and cross-sections were stained with Masson Trichrome (Figure 1A). This stains collagen dark blue, which can be quantified to determine relative interstitial fibrosis levels (Figure 1B).[28] Interstitial fibrosis increases with age and is a marker of the HCM phenotype[29]; however, there was no significant difference among the different time points or between the conditions (Figure 1C). The significant increase in the nontransgenic 6 month mice can be explained by low sample size (n=1). Therefore, there is no evidence for an increase in interstitial fibrosis in the mutant transgenic mice.

We then looked at tissue samples from the 9-month-old nontransgenic and transgenic mice by electron microscopy to determine if ultrastructural changes typically associated with HCM were present. We specifically looked for sarcomere disarray, changes in cell-cell junctions, and differences in protein aggregation. We again saw no significant differences between the nontransgenic and the mutant transgenic mice tissue: both had minimal to no sarcomere disorganization, minimal to no interruptions in cell-cell interactions and relatively equal levels of electron dense, amorphous, non-membrane bound structures resembling protein aggregation (Figure 2).

We also looked for typical signs of cardiac remodeling, through echocardiography and analysis of heart weight to body weight ratios. There was no significant difference in the heart rate to body weight ratios between the nontransgenic and mutant transgenic mice, indicating that there was no increase in heart size or fibrosis in the mutant hearts (Figure 3). Echocardiograms revealed no

differences in the heart structure typically seen in HCM patients; there was no difference in left ventricular mass, septum thickness, posterior wall thickness, left ventricular diameter, ejection fraction, and fractional shortening among the nontransgenic and the mutant transgenic mice ranging from 3 months to 12 months in age (Figure 3). Overall, we found that the mutant transgenic mice did not develop a disease phenotype at the tissue level or the organ level.

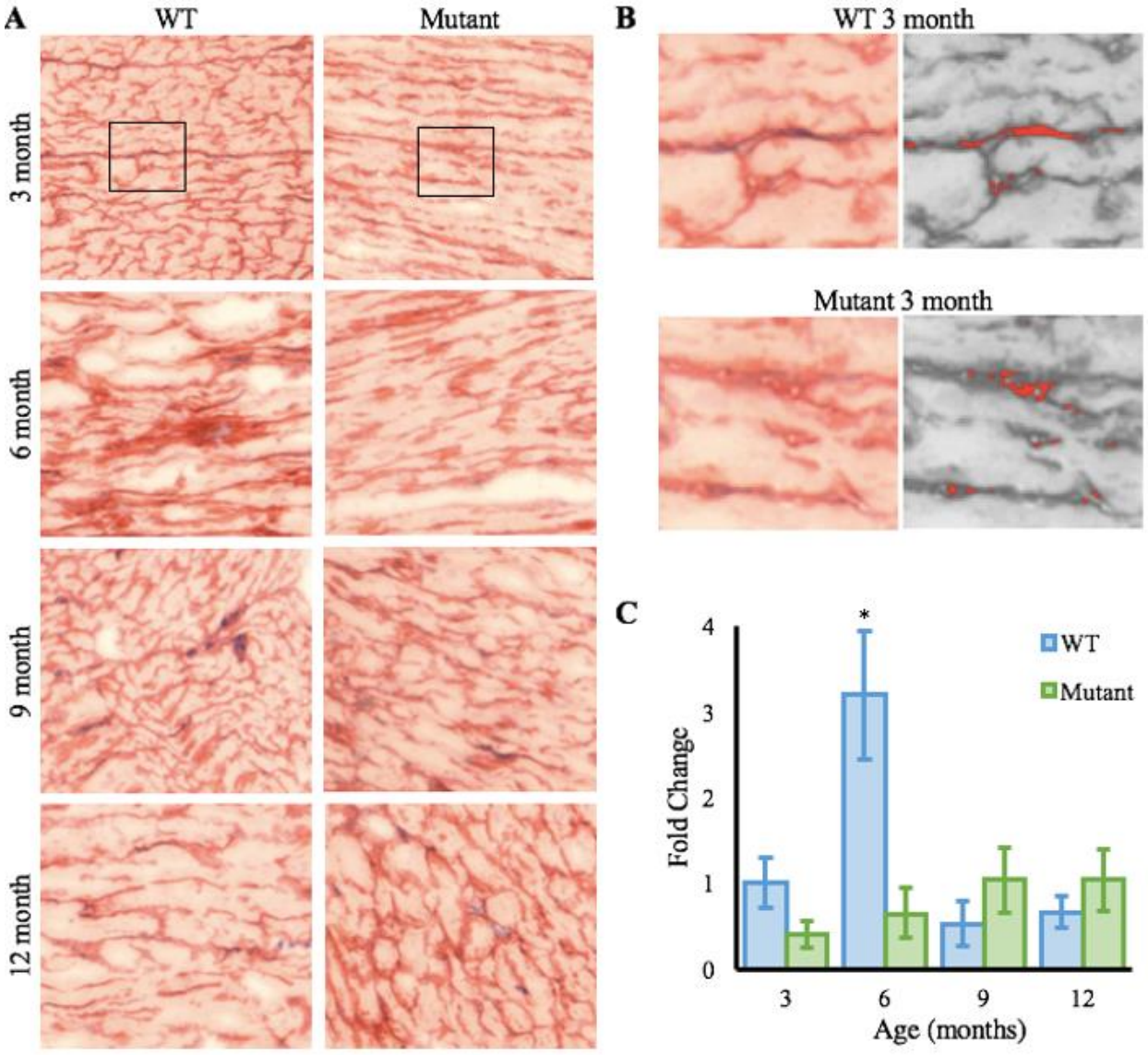

Figure 1: No difference in fibrosis in wild type and mutant mouse ventricular tissue
A) Ventricular tissue isolated from wild type and mutant mice ranging from three to twelve months old and stained with Masson's Trichrome stain. Muscle, erythrocytes and cytoplasm are stained red, collagen is stained blue and nuclei are stained dark brown. 20-30 20x images were taken across three tissue sections per mouse, n=1. B) Magnified image of the boxed regions in part A, left. Corresponding image from the ImageJ software used to quantify fibrosis; red indicates collagen, right. C) Quantification of fibrosis among the conditions and ages. One way ANOVA with Scheffe post-hoc analysis, *$p<0.05$

Staining by University of Michigan ULAM In-Vivo Animal Core, microscopy and analysis by Neha Hafeez.

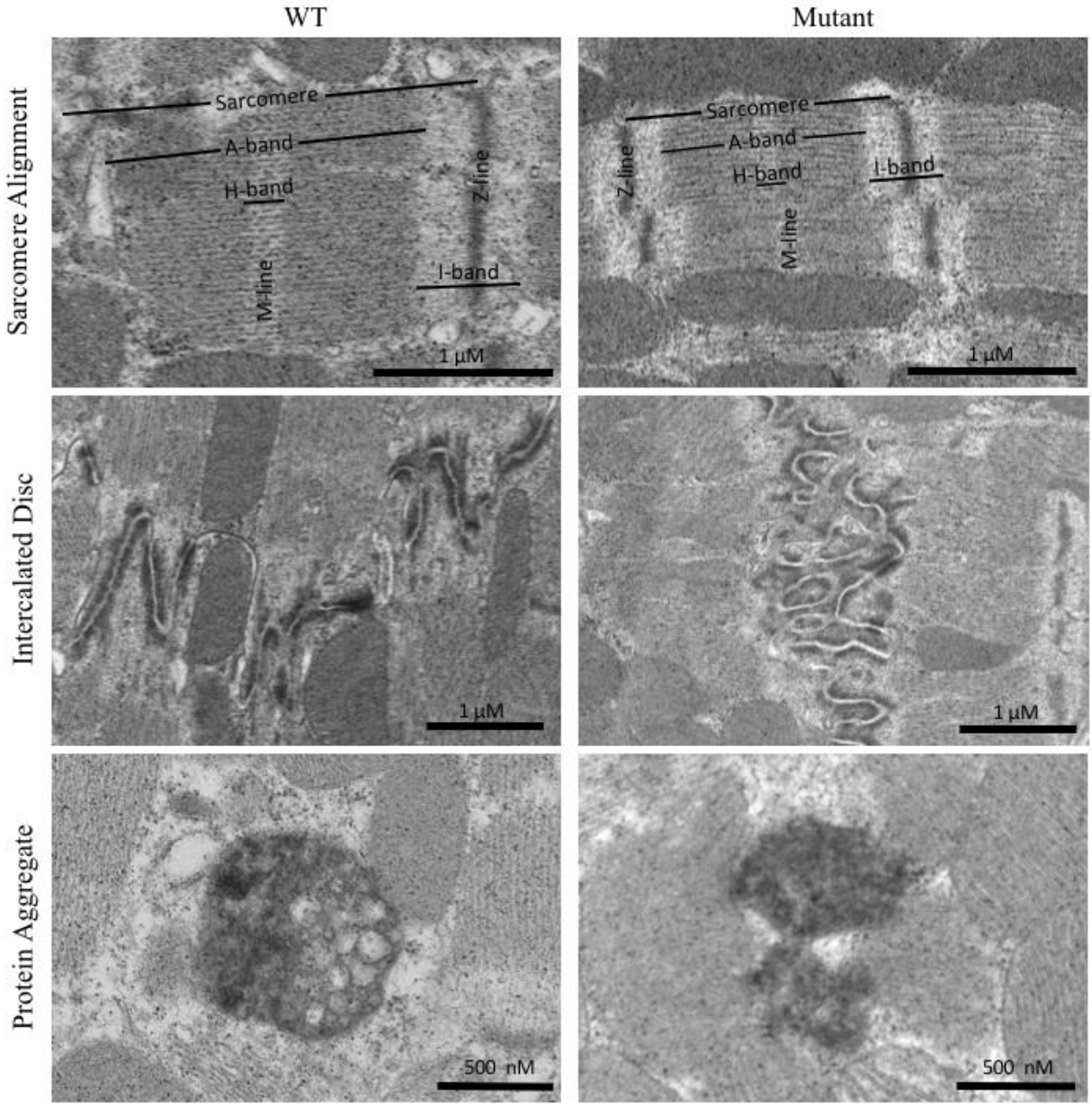

Figure 2: No ultrastructural difference in wild type and mutant mouse ventricular tissue analyzed via transmission electron microscopy (TEM)
Left ventricular tissue isolated from 9-month-old wild type and mutant mice was prepared for transmission electron microscopy. Representative images of sarcomere alignment, intercalated disc, and protein aggregates are shown. Images were qualitatively assessed.

Sample preparation by the University of Michigan Microscopy and Image Analysis Laboratory and microscopy by Neha Hafeez and Amelia Glazier.

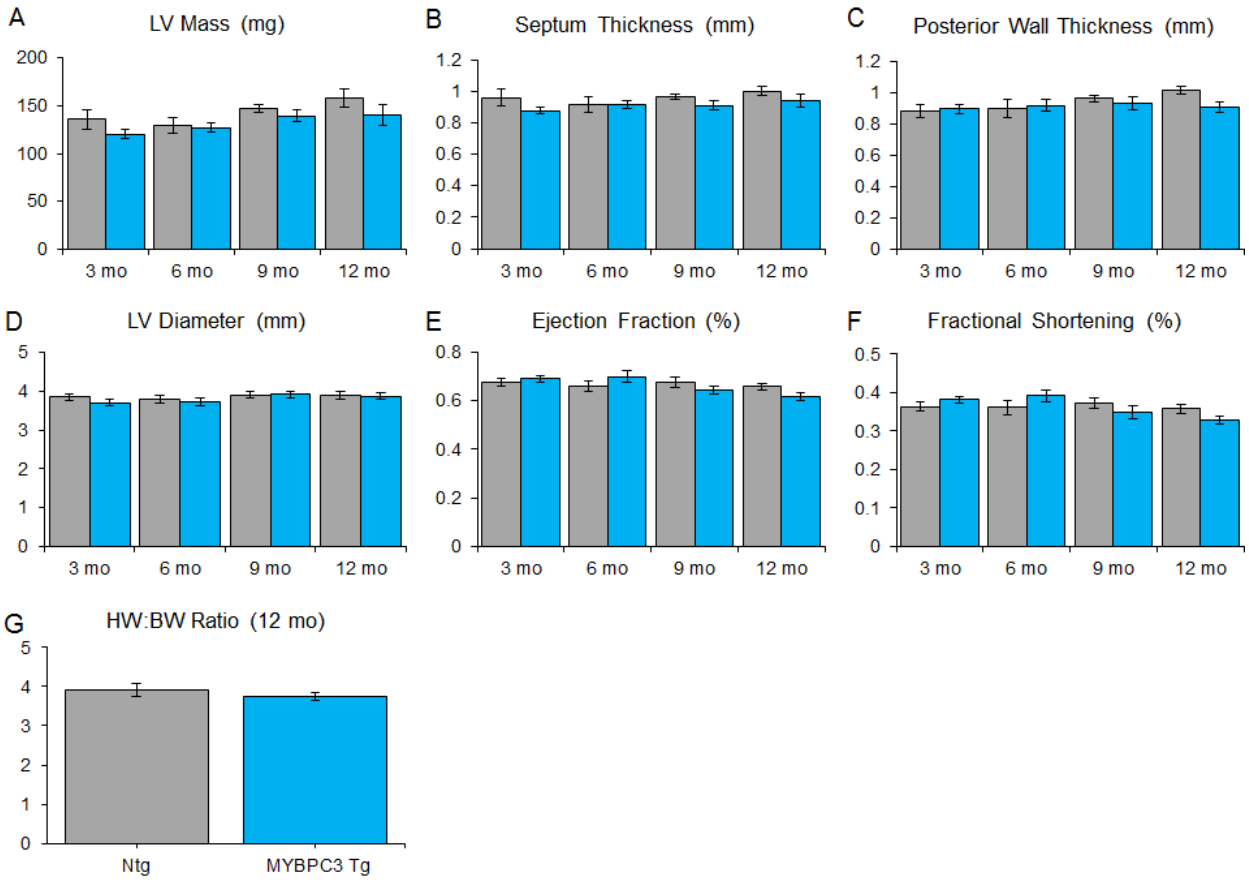

Figure 3: No structural or functional differences between the wild type and mutant transgenic mouse hearts

A-F) Data analysis from echocardiograms of wild type and transgenic mice ranging from 3 months to 12 months in age. G) Heart weight and body weight ratios of 12-month-old wild type and mutant mice were collected. n>10, independent samples t-test

Mouse collections done by Jaime Yob and Amelia Glazier; Echocardiography by the University of Michigan Frankel Cardiovascular Center Physiology and Phenotyping Core

Discussion

Due to the heterogeneity in the human clinical presentation of hypertrophic cardiomyopathy, it is very difficult to predict the disease phenotype based solely on the causative mutation.[3] By studying a transgenic mutant mouse model, we hoped to establish a method to characterize and analyze the genotype-phenotype interactions of various MYBPC3 mutations. We examined the mouse phenotype at the organ level via heart weight to body weight ratio analysis and echocardiograms and at the tissue level via fibrosis quantification and electron microscopy analysis. However, analysis at both levels showed no significant differences in interstitial fibrosis or structural disarray, indicating that the mice do not develop the HCM phenotype.

The mutant transgenic mice did not express the phenotype possibly due to cardiac and hemodynamic differences[3], including much faster heart rates (400-600 bpm in mice versus 75-180 bpm in humans) and differences in calcium handling[30] compared to humans. Additionally, the mice do not exhibit haploinsufficiency; unlike in human patients, the endogenous wild type alleles may provide sufficient protein expression for normal function in the mice. With the transgenic model, the mutant protein is expressed under a different promoter than the endogenous protein, resulting in mutant protein expression levels independent of the endogenous protein. Likewise, the mice could have some intrinsic compensatory mechanism that could either counteract the effects of the mutant transgene or could result in different protein dosages than expected.[31] After recognizing that this mouse model does not express the HCM phenotype, I switched my focus to characterizing the mutations in primary cardiomyocytes. The cell-based model also allows us to examine many different mutation types under acute expression conditions.

Part 2: Cell Based Model of Hypertrophic Cardiomyopathy

Results

MYBPC3 Truncated Proteins Unstably Express and Mislocalize In Vitro

We created WT and mutant human MYBPC3 constructs containing an N-terminal FLAG epitope tag that express in neonatal rat ventricular cardiomyocytes (NRVMs) via adenoviral transduction. The mutations span the length of MYBPC3 and are found in HCM patients.[32] The Ile154Leufs*5, c.2905+1G>A, Asp1076Valfs*6, and Trp1098* are nonsense mutations in the C0-C1 linker, C7, C8-C9 linker, and C10 domain, respectively. Localization patterns and expression levels were analyzed via immunofluorescence and western blot analysis. We used a micropatterning technique of printing fibronectin on PDMS coverslips to constrain the NRVMs to 20 μM wide rows, forcing the myocytes into a more adult-like rod shape (Figure 4D).[15] This technique allowed us to better visualize the sarcomere organization and subcellular localization of the mutant protein. FLAG-WT localized correctly to the thick filament C-zone. Ile154Leufs*5 localized in the nucleus and the other truncated proteins localized diffusely in the cytosol (Figure 4A). The Ile154Leufs*5 and c.2905+1G>A mutants showed significantly reduced MYBPC3 protein expression compared to the FLAG-WT (Figure 4C).

MYBPC3 C3 Domain Non-Truncated Proteins Localize Normally and MYBPC3 C10 Domain Non-Truncated Proteins Mislocalize In Vitro and Unstably Express

We created non-truncating human MYBPC3 constructs containing an N-terminal FLAG epitope tag that express in NRVMs via adenoviral transduction. The Arg495Gln, Arg502Trp, and Phe503Leu are missense mutations in the C3 domain. The Leu1238Pro is a missense mutation and the Gly1248_Cys1253Dup contains an in-frame duplication in the C10 domain. These mutations are also found in HCM patients. Using the same micropatterning technique described above, immunofluorescent analysis showed correct localization of the Arg495Gln, Arg502Trp, and

Phe503Leu to the thick filament C-zone, similar to the FLAG-WT. However, the Leu1238Pro and Gly1248_Cys1253Dup both localized diffusely in the cytosol (Figure 5A). Lower exposure levels were used to quantify protein expression of the Arg495Gln, Arg502Trp, and Phe503Leu (Figure 5B), but higher exposure levels were necessary to quantify protein expression of the Leu1238Pro and Gly1248_Cys1253Dup mutant proteins (Figure 5C). The Arg495Gln, Phe503Leu, Leu1238Pro, and Gly1248_Cys1253Dup mutants showed significantly reduced MYBPC3 protein expression compared to the FLAG-WT (Figure 5D).

MYBPC3 Interacts with Hsp70 Family Protein Chaperones

Purified WT, Ile154Leufs*5 and Trp1098* FLAG-MYBPC3 transduced NRVM lysates were analyzed via co-immunoprecipitation and mass spectrometry (LC-MS/MS) to determine MYBPC3 binding partners. Spectral counts of interacting proteins were normalized to abundance of the FLAG-MYBPC3 bait protein in each individual sample. Heat shock cognate 70 kDa (Hsc70/*Hspa8*) and the stress-inducible heat shock protein (Hsp70/*Hspa1a*) were found to be the most abundant chaperone interactors with the WT MYBPC3 (Figure 6A). Several proteins involved in other cellular functions, including metabolism and protein translation, were also found. Interestingly, the normalized spectral counts for the Hsp70 and Hsc70 varied between MYBPC3 mutations. The Ile154Leufs*5 had the lowest spectral counts for Hsp70 and Hsc70 and Trp1098* had the highest spectral counts relative to the WT immunoprecipitates (Figure 6B). Such differences could be indicative of a loss of chaperone binding domains or structural changes affecting chaperone interactions.

MYBPC3 Protein Degradation Impeded by Hsc70 Knockdown

In addition to aiding in protein folding, Hsp70 family protein chaperones are known to interact with E3 ubiquitin ligases, linking Hsp70 function to substrate ubiquitination and UPS-mediated degradation.[33] Therefore, to better understand the role of the Hsp70 family proteins and their interaction with the mutant MYBPC3 proteins, we analyzed the effects of Hsc70 knockdown on MYBPC3 degradation rates by cycloheximide pulse-chase assays. The cycloheximide inhibited *de novo* protein synthesis, allowing for protein degradation to be measured over time. NRVMs were incubated with either the scrambled siRNA control or the Hsc70 siRNA against rat *Hspa8*, which effectively reduced Hsc70 protein expression by 40-50% (data not shown). MYBPC3 protein levels were measured by western blots. The Hsc70 siRNA knockdown resulted in a significantly decreased protein degradation rate for the FLAG-WT, Trp1098* (Figure 7C), and Gly1248_Cys1253Dup (Figure 8C) MYBPC3 proteins compared to the scrambled siRNA control condition. The Hsc70 siRNA knockdown did not significantly affect degradation rates of the Ile154Leufs*5 (Figure 7B) or Arg495Gln (Figure 8B). Preliminary results using Arg502Trp also indicate no difference in degradation rates with Hsc70 knockdown (data not shown). Expression levels of other sarcomere proteins, α-actinin (Figure 7 and 8) and myosin heavy chain (data not shown), were also measured to ensure that the degradation rates measured for MYBPC3 were not just due to general turnover of all sarcomere proteins. Western blot data was fitted to first-order exponential decay curves; WT and mutant MYBPC half-lives were calculated from the resulting fit parameters (Table 1).

MYBPC3 Protein Degradation Accelerated by Hsp70 Activation

To examine the effects of Hsp70/Hsc70 activation, we used the small molecule YM-1, which stabilizes Hsp70 and Hsc70 in their ADP-bound conformation.[34] The ADP-bound state of Hsp70 has a tighter affinity for its substrates compared to the ATP-bound state.[35] Cycloheximide pulse-chase experiments were repeated with NRVMs incubated with Hsp70 activator YM-1 or the

DMSO vehicle for 24 hours. Hsp70 activation resulted in a significantly increased MYBPC3 protein degradation rate for the WT and all of the mutant proteins (Figure 7D-F, Figure 8D-F). Again, the MYBPC3 degradation rate is different from that of α-actinin (Figure 7-8) and myosin heavy chain (data not shown). The degradation rates were fitted to first-order exponential decay curves; WT and mutant MYBPC half-lives were calculated from the resulting fit parameters (Table 1).

C10 domain non-truncating MYBPC3 mutants degrade at a faster rate than C3 domain non-truncating MYBPC3 mutants.

Protein degradation rates were determined via cycloheximide pulse chase experiments and AlphaLISA analysis. C3 domain non-truncating mutants were expressed at MOI 2 and C10 domain non-truncating mutants were expressed at MOI 10 due to significantly lower expression levels. We found that the half-life of the C3 domain mutants were significantly greater than the WT MYBPC3 protein (14.85 hours and 14.88 hours for the Arg495Gln and Arg502Trp respectively compared to 6.70 hours for the WT protein) (Figure 9A). Conversely, the half-lives for the C10 domain mutants were significantly lower than the WT MYBPC3 protein (2.24 hours and 0.77 hours for the Glu1248_Cys1253Dup and Leu123Pro respectively compared to 11.13 hours for the WT) (Figure 9B). It is interesting that the WT MYBPC3 protein has a much higher half-life when expressed at MOI 10 compared to MOI 2; this could be potentially due to added stress on the proteasome to clear unincorporated MYBPC3, resulting in slower overall degradation rates. Regardless, the half-life of the C10 non-truncating mutant protein is much shorter, indicating that the protein is much less stable compared to the WT and the C3 domain non-truncation mutant proteins.

Mutant MYBPC3 Expression Does Not Result in Hsc70 Nuclear Translocation

The Hsp70 family proteins have a highly-conserved function of localizing to the nucleus in response to cell stress and cell growth.[36,37] To examine whether the introduction of mutant MYBPC3 protein resulted in protein folding stress to the cell, we assessed Hsp70 and Hsc70 expression levels and localization. There was no change in Hsp70 or Hsc70 expression levels for any of the FLAG-tagged WT or mutant MYBPC3 compared to the control (Figure 10A,B). Hsp70 levels were upregulated only in the cells that were heat shocked for 1 hour at 45°C, as expected (Figure 10A). To determine if MYBPC3 mutants affected nuclear localization of Hsc70, we performed colocalization analysis using Hsc70 and DAPI immunostains. Using confocal microscopy, we created a three-dimensional rendering of the nuclei of each of the mutants and analyzed the percentage of the Hsc70 signal within the DAPI signal volume. We also calculated the average Mander's correlation coefficient, which is another quantitative measurement of colocalization. We found that nuclear localization of Hsc70 was not significantly different among the transduced and control cells; Hsc70 nuclear localization was only increased in the heat shock condition. Therefore, mutant MYBPC3 expression is not associated with stress-induced Hsp70 expression or Hsc70 nuclear translocation, suggesting that truncated MYBPC3 mutations do not induce protein folding stress.

Wild type MYBPC3 not detected in human Arg502Trp ventricular myocardial tissue

Ventricular myocardial tissue from a patient with the Arg502Trp MYBPC3 mutation was collected during a septal myectomy procedure and non-failing ventricular myocardial tissue was collected from unmatched donor hearts. WT and mutant MYBPC3 protein levels in the tissues were analyzed by mass spectrometry. Interestingly, wild type MYBPC3 protein could not be found in the Arg502Trp myocardial tissue, even though it could be detected in the non-failing heart tissue. Our lab previously reported that in human Arg495Gln mutants, the mutant to wild type MYBPC3

protein level was about 2:1.[32] This suggests an allelic imbalance for the Arg502Trp and the Arg495Gln mutations, possibly indicating that these mutant proteins are better able to incorporate into the sarcomere or are more resistant to degradation compared to WT MYBPC3.

Our lab also previously reported that truncated mutant proteins were not detectable via mass spectrometry analysis among any of human mutant myocardial tissue tested, suggesting that the truncated mutants are highly unstable and unable to incorporate into the sarcomere.[32]

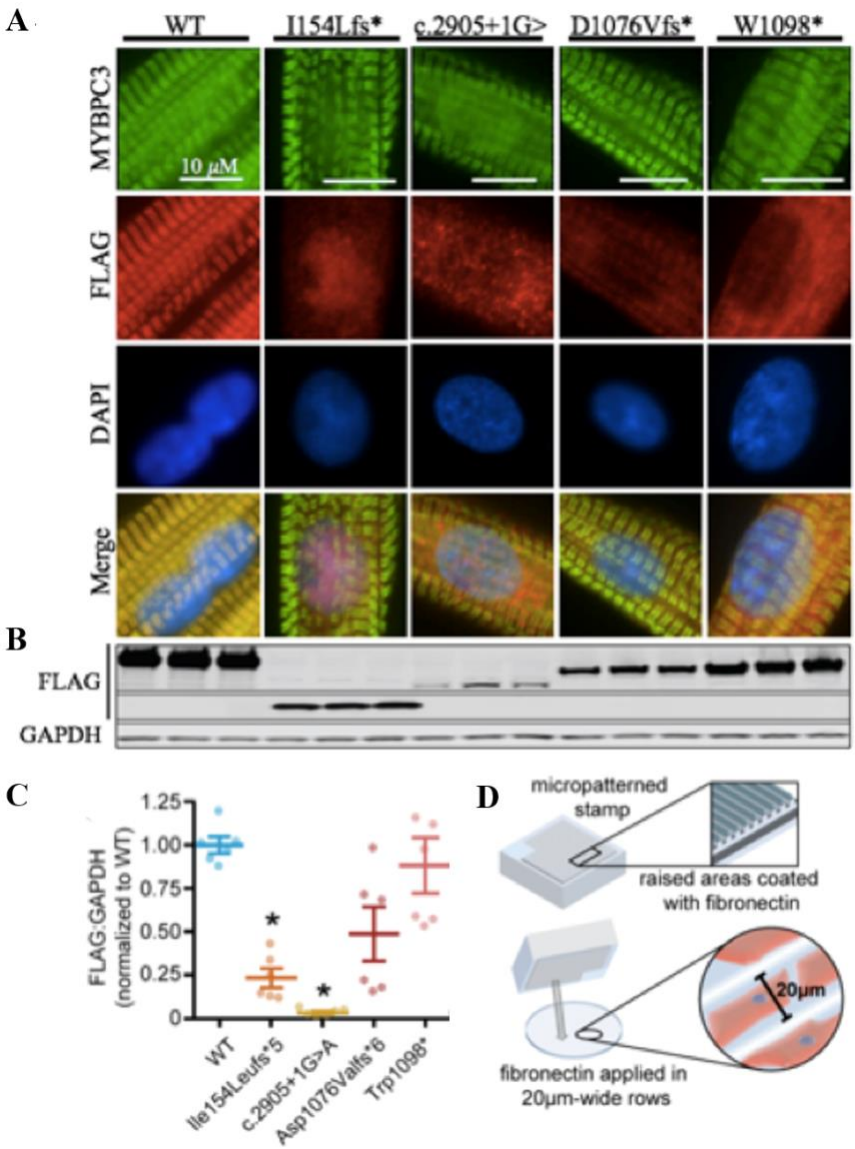

Figure 4: FLAG-tagged WT and truncating mutant MYBPC3 constructs expressed in NRVMs via adenoviral transduction

A) FLAG-WT MYBPC3 correctly localizes to the sarcomere C-zone in patterned NRVMs, while FLAG-I154Lfs* MYBPC3 mislocalizes to the nucleus and the other MYBPC3 mutants mislocalize diffusely in the cytosol. Immunofluorescence images, 60X magnification, scale bar = 10 μM. B) Representative western blots of FLAG-MYBPC3 expression levels. C) Quantification of western blot results, mean ± SEM, $p<0.05$, One way ANOVA. D) Diagram depicting micropatterning technique.

Constructs created by Vi Tang and Adam Helms, immunofluorescence and microscopy by Neha Hafeez, western blots by Amelia Glazier.

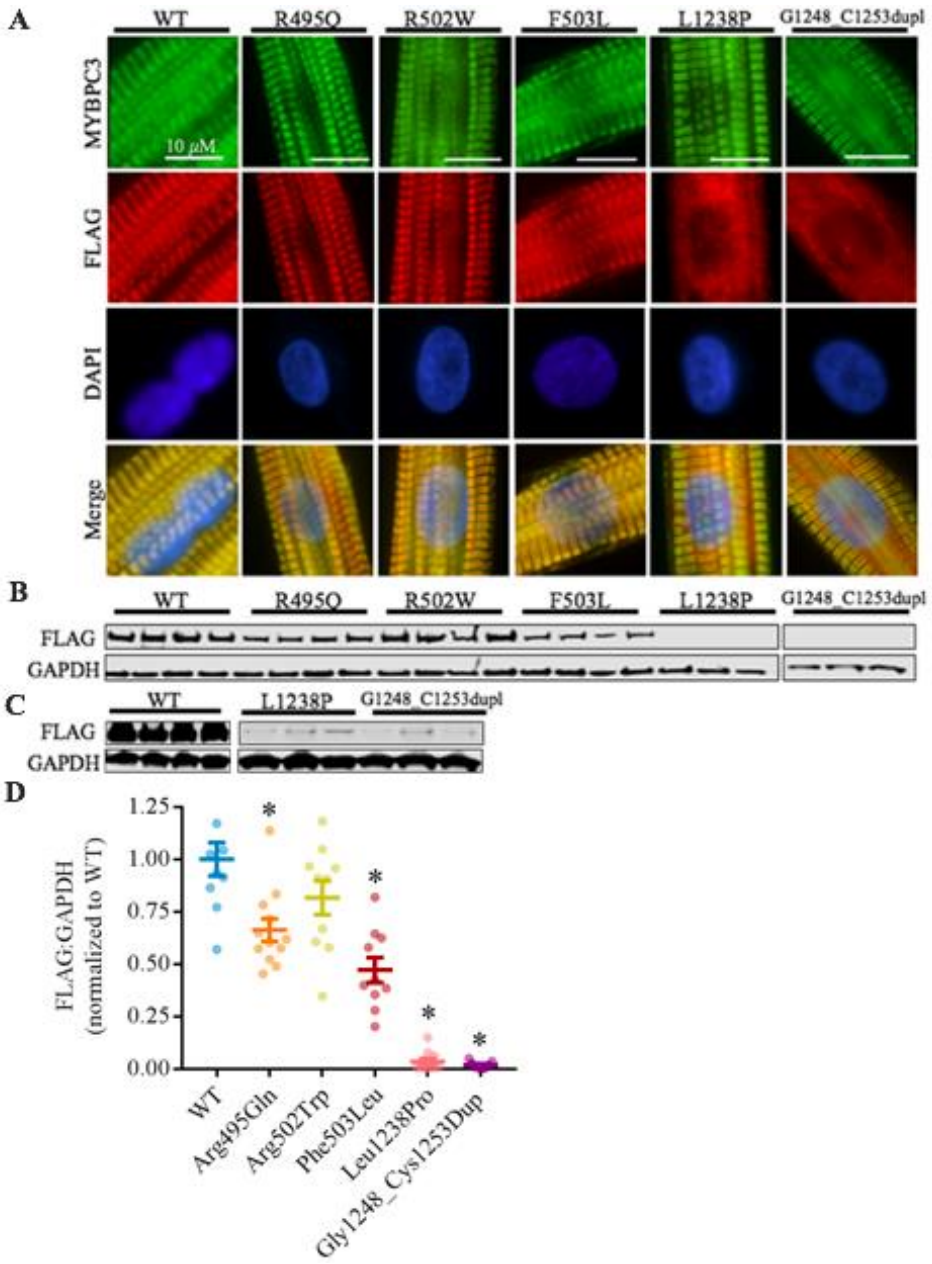

Figure 5: FLAG-tagged WT and non-truncating mutant MYBPC3 constructs expressed in NRVMs via adenoviral transduction

A) FLAG-WT MYBPC3, FLAG-Arg495Gln MYBPC3, FLAG-Arg502Trp MYBPC3 and FLAG-Phe503Leu MYBPC3 correctly localize to the sarcomere C-zone in patterned NRVMs, while FLAG-Leu1238Pro MYBPC3 and FLAG-Gly1248_Cys1253Dup MYBPC3 mislocalize diffusely in the cytosol. Immunofluorescence images, 60X magnification, scale bar = 10 μM. B) Representative western blots of FLAG-MYBPC3 expression levels. C) Higher exposure western blot to show expression of the lower expression mutant proteins. D) Quantification of western blot results, mean ± SEM, *$p<0.05$, One way ANOVA with Post-hoc Scheffe test.

Constructs created by Neha Hafeez and Vi Tang, immunofluorescence and microscopy by Neha Hafeez, western blots by Neha Hafeez.

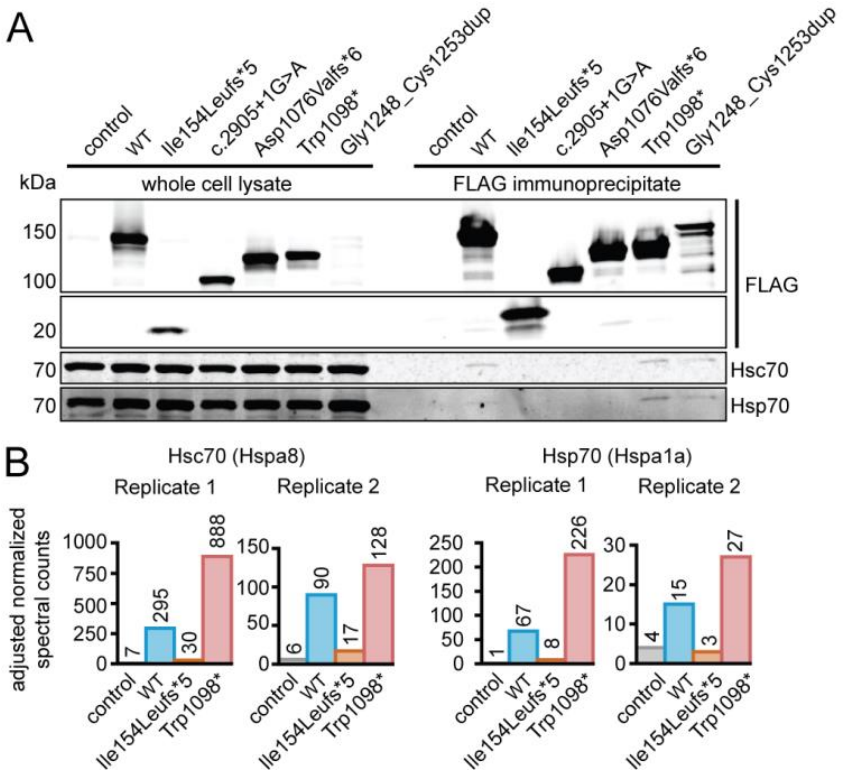

Figure 6: MYBPC3 interacts with Hsc70 and Hsp70
A) Co-immunoprecipitation experiment of Hsc70 and Hsp70 with FLAG-tagged WT and mutant MYBPC3. Western blots from whole cell lysate, left panel and from FLAG immunoprecipitates, right panel. Loss of Hsc70 and Hsp70 interaction with the Ile154Leufs*5, c.2905+1G>A, and Asp1076Valfs*6 FLAG-MYBPC3 mutants. B) Adjusted spectral counts for Hsc70 and Hsp70 normalized to abundance of the WT or mutant FLAG-MYBPC3 bait protein. Enrichment of Hsc70 and Hsp70 in FLAG-WT and FLAG-Trp1098* MYBPC3.

Immunoprecipitation experiments and analysis by Amelia Glazier; mass spectrometry (LC-MS/MS) and proteomics analysis by the University of Michigan Pathology Proteomics Core (Dattatreya Mellacheruvu PhD, Venkatesha Basrur PhD, and Alexey Nesvizhskiy PhD)

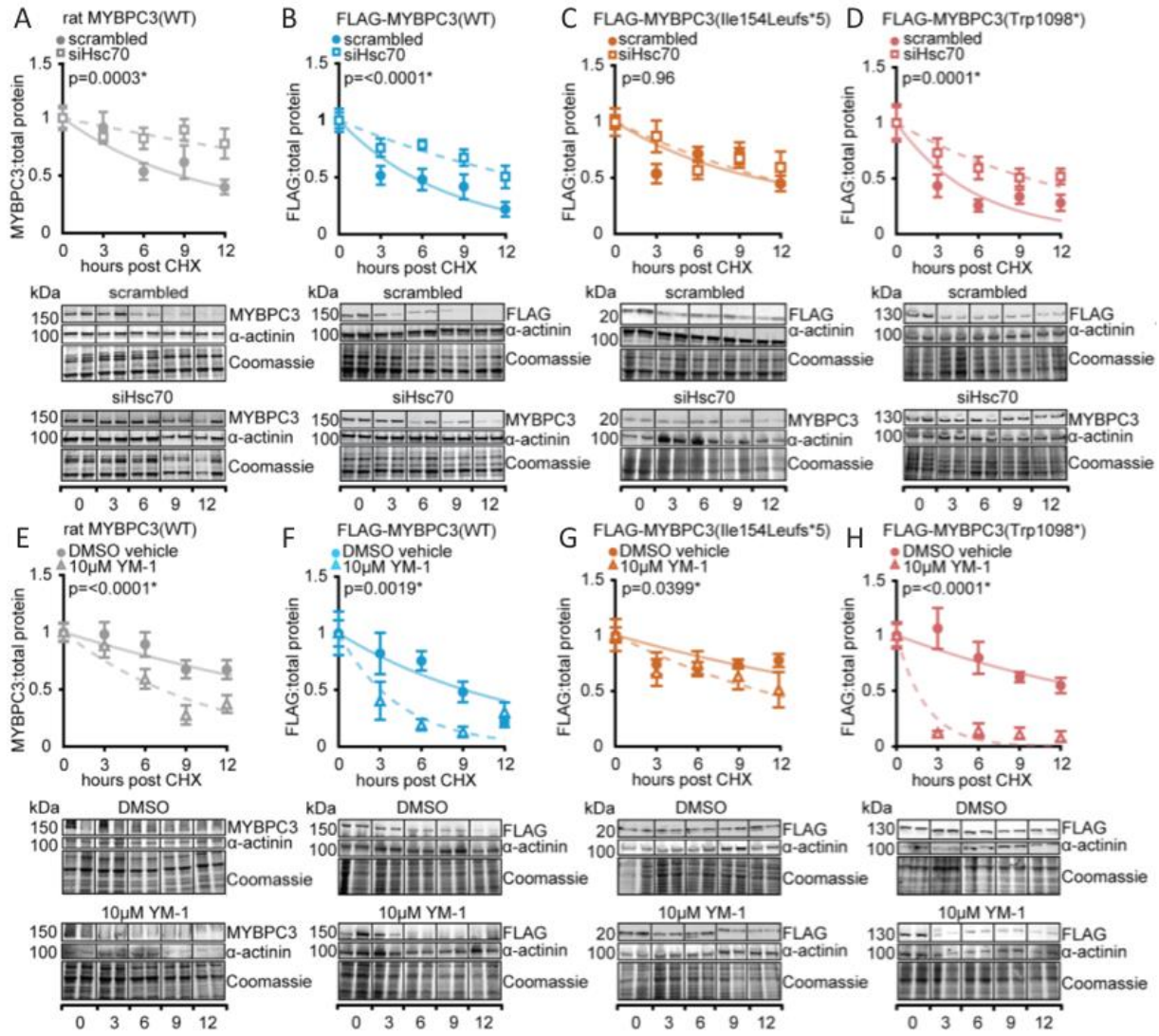

Figure 7: WT and Truncated Mutant MYBPC3 degradation rates affected by Hsc70 Knockdown and Hsp70 Activation via YM-1 Treatment

Degradation rates were fitted to first-order exponential decay equations. A-D) MYBPC3 protein degradation rate is slower with Hsc70 siRNA treatment (dashed lines, open squares) compared to scrambled control siRNA treatment (solid line, solid circles). E-H) MYBPC3 protein degradation rate is faster with YM-1 treatment (dashed lines, open triangles) compared to the DMSO vehicle control (solid lines, solid squares). Representative western blots shown each figure. n≥7, Mean ± SEM, p values represent significance of comparison of fit parameter reaction constant k between conditions.

CHX chase experiment and western blot analysis by Amelia Glazier.

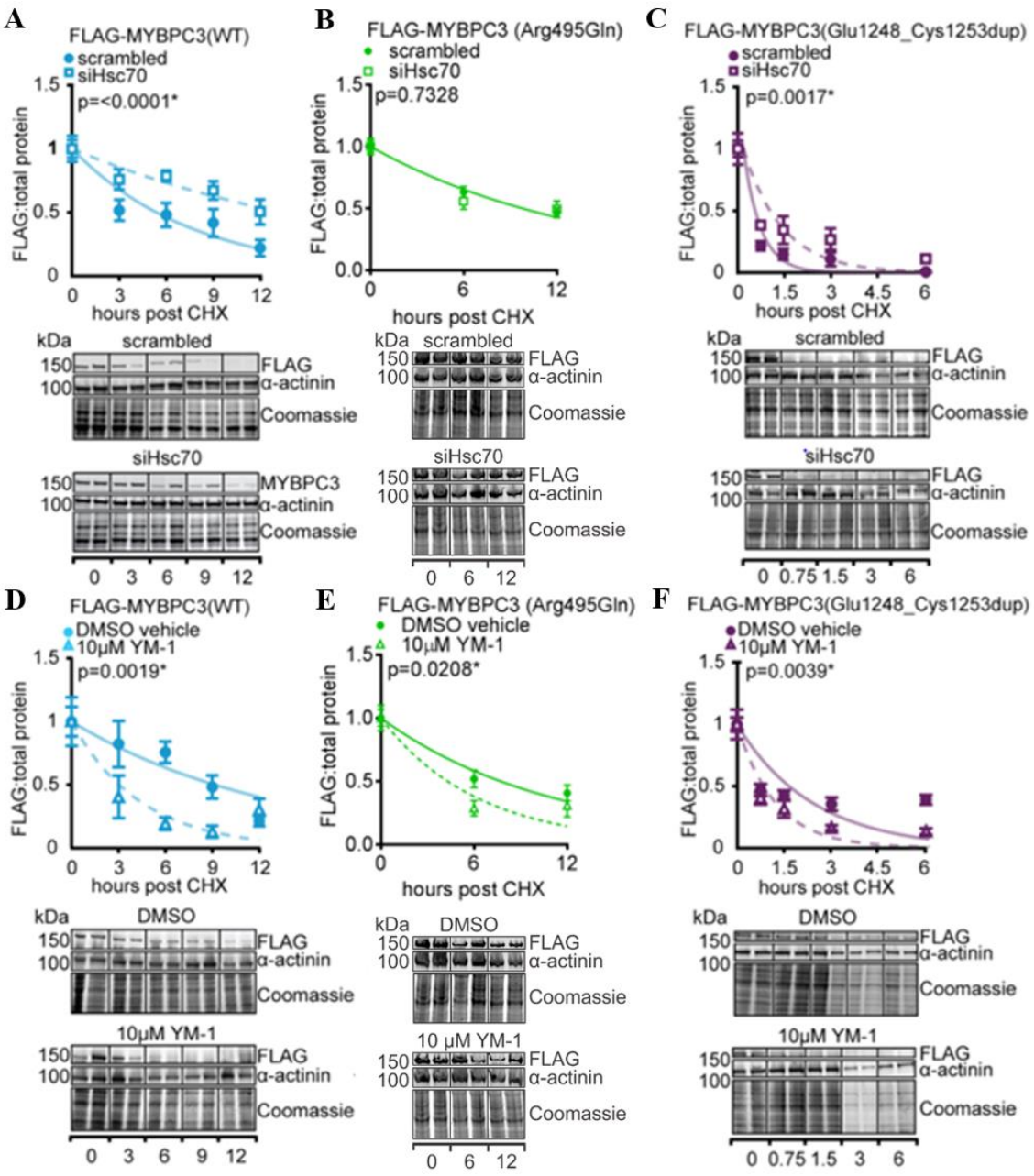

Figure 8: WT and Non-Truncated Mutant MYBPC3 degradation rates affected by Hsc70 Knockdown and Hsp70 Activation via YM-1 Treatment

Degradation rates were fitted to first-order exponential decay equations. A-D) MYBPC3 protein degradation rate is slower with Hsc70 siRNA treatment (dashed lines, open squares) compared to scrambled control siRNA treatment (solid line, solid circles) for the FLAG-WT and Gly1248_Cys1253Dup. E-H) MYBPC3 protein degradation rate is faster with the YM-1 incubation (dashed lines, open triangles) compared to the DMSO vehicle control (solid lines, solid squares). Representative western blots shown each figure. n≥7, Mean ± SEM, p values represent significance of comparison of fit parameter reaction constant *k* between conditions.

CHX chase experiment and western blot analysis by Neha Hafeez and Amelia Glazier.

Table 1. Kinetic Fit Parameters

	treatment	$t_{½}$ (hr)	$t_{½}$ 95% CI (hr)	k (hr^{-1}) ± SE	p-value for fit comparison vs respective control
rat MYBPC3 (WT)	scrambled siRNA	8.37	7.26 to 9.88	0.828±0.013	0.0003*
	Hsc70 siRNA	27.0	19.9 to 41.6	0.0257±0.0090	
	DMSO vehicle	18.8	16.0 to 22.8	0.0368±0.0064	<0.0001*
	10μM YM-1	7.02	6.26 to 7.99	0.0988±0.012	
FLAG-MYBPC3 (WT)	scrambled siRNA	5.42	4.76 to 6.31	0.129±0.018	<0.0001*
	Hsc70 siRNA	13.3	11.5 to 15.7	0.0522±0.0080	
	DMSO vehicle	8.45	7.11 to 10.4	0.0821±0.015	0.00019*
	10μM YM-1	2.97	2.33 to 4.10	0.233±0.064	
FLAG-MYBPC3 (Ile154Leufs*5)	scrambled siRNA	11.3	9.52 to 13.8	0.0615±0.011	0.96
	Hsc70 siRNA	11.2	9.53 to 13.4	0.0622±0.011	
	DMSO vehicle	20.3	16.1 to 26.6	0.0342±0.0085	0.040*
	10μM YM-1	10.3	8.67 to 12.6	0.0674±0.013	
FLAG-MYBPC3 (Trp1098*)	scrambled siRNA	4.24	3.77 to 4.85	0.163±0.020	0.0001*
	Hsc70 siRNA	9.72	8.43 to 11.5	0.0713±0.011	
	DMSO vehicle	15.3	12.3 to 20.0	0.0454±0.011	<0.0001*
	10μM YM-1	1.33	1.10 to 1.69	0.521±0.11	
FLAG-MYBPC3 (Arg495Gln)	scrambled siRNA	10.06	8.03 to 12.85	0.069±0.008	0.733
	Hsc70 siRNA	9.46	7.20 to 12.71	0.0733±0.0099	
	DMSO vehicle	7.69	5.75 to 10.44	0.090±0.013	0.0208*
	10μM YM-1	4.29	2.65 to 6.5	0.161±0.031	
FLAG-MYBPC3 (Glu1248_Cys1253dup)	scrambled siRNA	0.395	0.330 to 0.493	1.75±0.35	0.0017*
	Hsc70 siRNA	0.997	0.848 to 1.13	0.715±0.10	
	DMSO vehicle	1.68	1.49 to 1.93	0.412±0.053	0.0040*
	10μM YM-1	0.844	0.735 to 0.992	0.821±0.12	

Table 1: Kinetic Fit Parameters
First-order exponential decay curve fitting parameters from the cycloheximide chase assay results shown in Figures 7-8.

CHX chase experiment and western blot analysis by Neha Hafeez and Amelia Glazier.

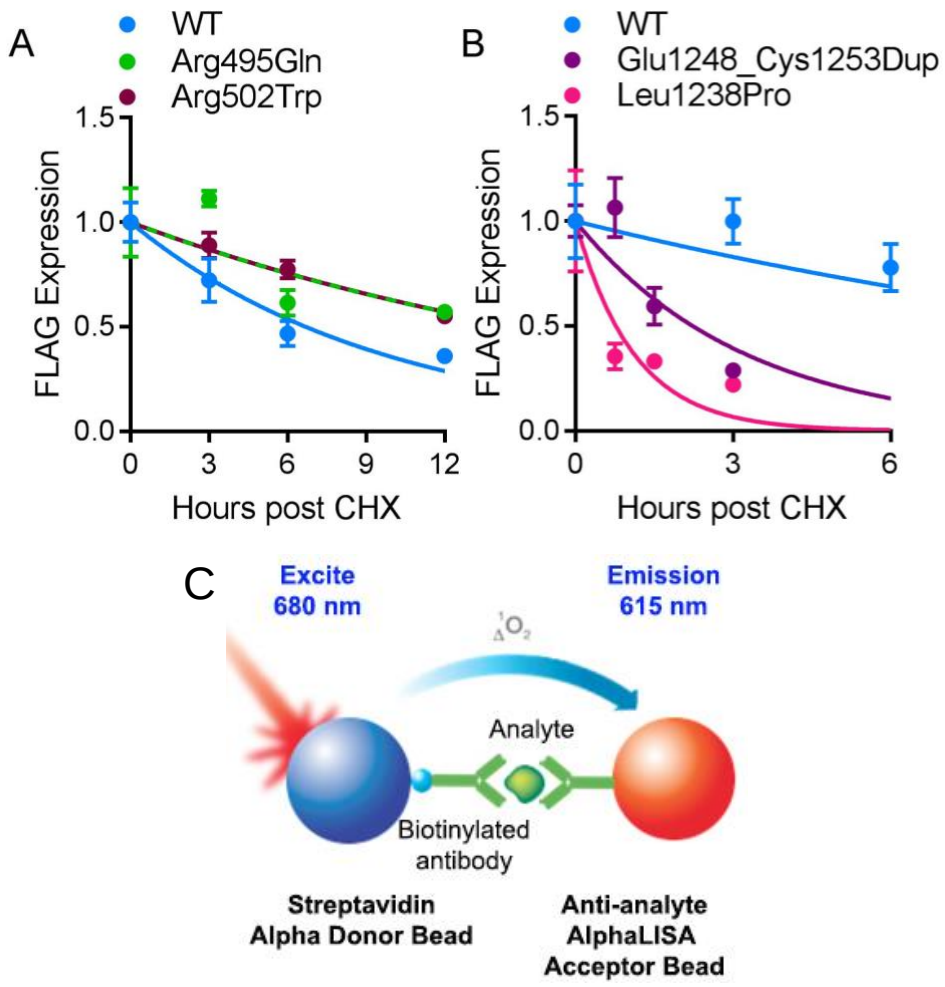

Figure 9: C3 domain non-truncating MYBPC3 mutants have a longer half-life than C10 domain non-truncating MYBPC3 mutants

FLAG expression of NRVM samples from cycloheximide pulse-chase experiment with no treatment was quantified via AlphaLISA analysis. A) MYBPC3 C3 domain non-truncating mutations were expressed at MOI 2. B) MYBPC3 C10 domain non-truncating mutations were expressed at MOI 10 because the Glu1248_Cys1253Dup and Leu1238Pro MYBPC3 mutant proteins were undetectable at MOI 2. n=3, Mean ± SEM, p values represent significance of comparison of fit parameter reaction constant *k* between conditions (*$p<0.05$). C) Depiction of AlphaLISA principle (adapted from Perkin Elmer).

CHX Chase assay, AlphaLISA experiment, and analysis by Neha Hafeez.

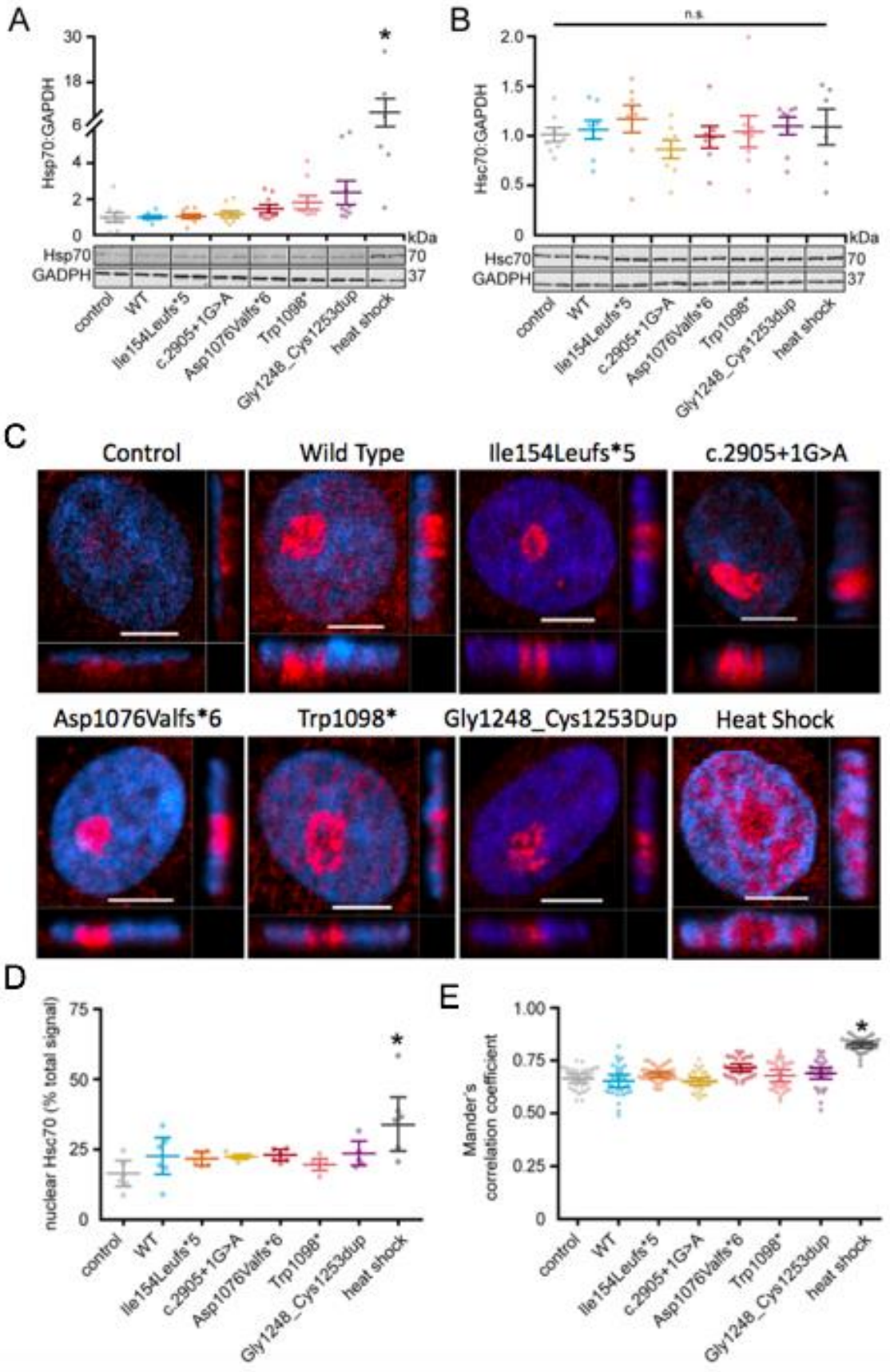
A
Hsp70:GAPDH
30
18
6
4
2
0
*
kDa
Hsp70
GADPH
70
37
control
WT
Ile154Leufs*5
c.2905+1G>A
Asp1076Valfs*6
Trp1098*
Gly1248_Cys1253dup
heat shock
B
n.s.
Hsc70:GAPDH
2.0
1.5
1.0
0.5
0
kDa
Hsc70
GADPH
70
37
control
WT
Ile154Leufs*5
c.2905+1G>A
Asp1076Valfs*6
Trp1098*
Gly1248_Cys1253dup
heat shock
C
Control
Wild Type
Ile154Leufs*5
c.2905+1G>A
Asp1076Valfs*6
Trp1098*
Gly1248_Cys1253Dup
Heat Shock
D
nuclear Hsc70 (% total signal)
75
50
25
0
*
control
WT
Ile154Leufs*5
c.2905+1G>A
Asp1076Valfs*6
Trp1098*
Gly1248_Cys1253dup
heat shock
E
Mander's correlation coefficient
1.00
0.75
0.50
0.25
0
*
control
WT
Ile154Leufs*5
c.2905+1G>A
Asp1076Valfs*6
Trp1098*
Gly1248_Cys1253dup
heat shock

Figure 10: Mutant MYBPC3 expression does not result in Hsc70 Nuclear Translocation
A-B) Quantification and representative western blots for Hsp70 and Hsc70 protein expression in NVRMs transduced with the FLAG-tagged WT and mutant MYBPC3. Kruskal-Wallis one way ANOVA $p=0.003$ and $p=0.48$ for Hsp70 and Hsc70, respectively. *$p<0.05$ vs control, Dunn's multiple comparisons test. C) Representative confocal images of the patterned NRVMs immunostained for Hsc70 and DAPI. 60X magnification, 5-6 nuclei per z-stack, 3 random fields selected. D) Hsc70 signal percentage within the DAPI signal volume. Kruskal-Wallis one way ANOVA $p=0.21$. $p<0.05$ vs control, Dunn's multiple comparisons test. D) Mander's correlation coefficient between DAPI and Hsc70 signals. Kruskal-Wallis one-way ANOVA $p<0.0001$. *$p<0.05$ vs control, Dunn's multiple comparisons test. Mean ± SEM.

Hsc70/Hsp70 Quantification by Amelia Glazier, Immunofluorescence and confocal microscopy by Neha Hafeez, Nuclear Hsc70 Quantification by Amelia Glazier, Mander's Correlation Coefficient Analysis by Neha Hafeez.

Discussion

In this study, we aimed to determine the effects of mutation type and location on the mechanism of pathogenesis. Analysis of the Sarcomeric Human Cardiomyopathy Registry (SHaRe) showed that truncating MYBPC3 mutants found in human HCM patients occurred throughout the length of the gene. However, the non-truncating mutations were found to cluster in the C3, C6, and C10 domains. This indicates that the mutation location may play an important role in HCM pathogenesis. All of the truncating and non-truncating mutations did not necessarily follow similar patterns, implying that the disease mechanisms are more complex than the previously published haploinsufficiency or "poison peptide" hypotheses.[20] The haploinsufficiency hypothesis states that the phenotype is due to insufficient protein levels within the sarcomere, whereas poison peptide hypothesis states that the mutant proteins act as dominant negative proteins and incorporate into the sarcomere myofilament.[21] We found that both the truncating and non-truncating mutations likely act via changes in both protein dosage and altered function, as indicated by differences in localization, expression, stability, and interactions with protein chaperones. This challenges the prevailing concept that the truncating MYBPC3 mutations are exclusively loss-of-function and supporting the haploinsufficiency hypothesis, and that the non-truncating MYBPC3 mutations are exclusively gain of function and supporting the poison peptide hypothesis.

All of the truncating mutants that I studied displayed mislocalization of the MYBPC3 mutant protein. The C0-C1 linker truncated protein localized to the nucleus and the rest of the mutant proteins (truncations in the C7 domain, C8-C9 linker, and C10 domain) localized diffusely in the cytosol. Such cytosolic mislocalization was also seen with the C10 domain non-truncating mutants. Mislocalization implies a loss-of-function scenario in which MYBPC3 cannot bind actin or myosin within the sarcomere. Conversely, the C3 domain non-truncating mutants localized normally

in the sarcomere C-zones, indicating that function is affected via an alternate mechanism, likely dominant-negative effects on contract, compared to the other C10 mutants.

If the truncating mutations exclusively result in loss-of-function, we would expect all of them to show reduced protein expression and stability. This is not the case for the longer truncating mutants which have protein levels similar to the WT protein or for the shorter length truncating mutant which showed a greater half-life than the WT protein (comparison of degradation rate with scrambled control siRNA treatment), although this could be explained by its sequestration in the nucleus. However, mass spectrometry results from patient tissues with truncating MYBPC3 mutations consistently fails to detect the presence of truncated protein. It remains unclear why these truncated mutants are relatively stable in an in vitro system given their aberrant localization and absence in human HCM tissue. However, this may suggest that the protein itself may not be less stable, but protein mislocalization could result in more rapid elimination.

Likewise, if the non-truncating mutations exclusively exert gain-of-function effects on contractility, we would expect all of them to incorporate into the sarcomere. However, the C10 domain non-truncating mutant proteins not only show diffuse cytosolic localization, but are expressed at much lower levels and are much less stable compared to the WT protein. This was an unexpected finding, but this may imply that an intact C terminus domain is necessary for proper protein incorporation and thus function. Regardless, these results suggest that there is more complexity to the mechanism of action beyond mutation type.

We also analyzed the different mutations to determine if there is a differential interaction of molecular chaperones and any consequent effects on protein degradation. Through co-immunoprecipitation and mass spectrometry analysis, we found that the Heat Shock Protein 70 kDa family of molecular chaperones interacts with MYBPC3. We then analyzed whether this interaction of Hsc70 with the mutant MYBPC results in differential general stress response due to variable

depletion of the Hsc70 pool in the cell. I had hypothesized that this could be the manner by which the mutations exhibit the poison peptide effect; however, I found that none of mutations result in a general stress response as indicated by no increase in nuclear Hsc70 translocation.[38]

We additionally examined the effect of Hsc70 knockdown and activation on MYBPC3 protein degradation. The WT and most of the mutant MYBPC3 proteins had a decreased degradation rate with Hsc70 knockdown and increased degradation rate with Hsc70 activation. This indicates that Hsc70 likely interacts with MYBPC3 to facilitate protein degradation. However, the degradation rates of the C3 domain non-truncated mutant proteins are not significantly affected by molecular protein chaperone Hsc70 knockdown. This suggests that these non-truncating mutations in the internal domains may enhance protein stability because they are not as susceptible to Hsc70 mediated degradation. This is supported by mass spectrometry results from human ventricular myocardial tissue of HCM patients with the Arg495Gln or Arg502Trp C3 domain non-truncating mutations. A 2:1 ratio of mutant MYBPC3 to wild type MYBPC3 was found in the Arg495Gln mutant patient tissue and wild type MYBPC3 could not even be detected in the Arg502Trp mutant patient tissue. This implies a gene dosage effect and that the possibly more stable C3 domain mutants outcompete the WT MYBPC3, supporting the poison peptide hypothesis. Unlike the C3 domain non-truncated mutants, the C10 domain non-truncated mutant MYBPC3 proteins appear to be less stable, mislocalize diffusely in the cytosol, and express at much lower levels than the WT MYBPC3, suggesting that the C10 missense mutations will act similarly to the truncating mutations and cause haploinsufficiency.

In conclusion, the various mutations show differences in localization, expression, stability, and interactions with molecular chaperones, implying that there may be some overlap of both the haploinsufficiency and poison peptide mechanisms in the pathogenesis of HCM. We additionally showed that C3 domain non-truncating mutations are more stable, potentially due to reduced

interaction with molecular chaperones and that the C10 domain non-truncating mutations are less stable, potentially due to interrupted C terminus domain activity. In the future, we hope to study the C6 domain non-truncating mutations to further dissect the role of mutation type and locus in the disease pathogenesis. Understanding the mechanisms by which the various mutations act can give insights into targeted therapy for HCM patients with these mutations in the future.

Materials and Methods

Masson trichrome staining & quantification

Ventricular tissue was isolated from wild type and mutant transgenic mice (expressing 75 kDa MYBPC3 truncating mutation in the C5 domain under the α-myosin heavy chain promoter on a background with two wild-type endogenous MYBPC3 alleles) ranging from three months to 12 months in age. Cross-sections were stained with Masson Trichrome stain and 20x images were taken over the entire tissue section (~30 images per tissue section) using a Nikon Eclipse Ti-E inverted microscope in brightfield under single-blind conditions. Images were loaded into ImageJ software using the RGB plugin to specifically detect levels of the collagen stain (blue). The data was analyzed by one-way ANOVA.

Mouse tissue sample preparation for transmission electron microscopy

Ventricular tissue was isolated from the nontransgenic and mutant transgenic mice. Samples were cut into roughly 2 by 2 mm pieces and processed for TEM analysis by the University of Michigan Microscopy and Image Analysis Laboratory (MIL).

Echocardiograms

Echocardiography done on nontransgenic and transgenic mice ranging from three months to twelve months in age performed under isoflurane anesthesia by the University of Michigan Frankel Cardiovascular Center Physiology and Phenotyping Core.

Mouse heart weight to body weight analysis

Body weights and heart weights of three-month-old wild type and mutant transgenic mice were collected. The data was analyzed by one-way ANOVA.

Animal Studies

All animal work was done with UCUCA approved protocols.

Isolation and culture of neonatal rat ventricular cardiomyocytes (NRVMs)

Ventricles of 1-3 day old neonatal rats were excised from Sprague-Dawley rats (Charles River) and carefully cut into smaller pieces. Ventricular tissue from approximately 10 pups were used during each cardiomyocyte isolation. After rinsing in ice-cold HBSS (Hank's Balanced Salt Solution), the tissue was pre-digested in 1 mg/mL trypsin (Worthington) at 4°C for 6 hours. The tissue was then further digested in 30 U/mL purified collagenase (Worthington), dissolved in Media 199 (Invitrogen) with Earle's salts, L-glutamine, 2.2 g/L sodium bicarbonate, 2% penicillin/streptomycin, 25mM HEPES, and 15% heat inactivated FBS (Invitrogen), in a Celstir® 50mL jacketed spinner flask (Wheaton) for 45 minutes at 37°C. Digested tissue was triturated using a 10 mL serological glass pipette, filtered through a 70μM cell strainer, and incubated for 20 minutes at room temperature for further digestion. The cells were then pre-plated on untreated plastic dishes for 1 hour at 37°C to reduce fibroblast contamination and filtered through a 40μM cell strainer. The cells were then put on plates coated with 5μg/mL bovine fibronectin (Sigma-Aldrich) or on fibronectin-micropatterned PDMS coverslips (see below) in maintenance media (Media 199 with Earle's salts, L-glutamine, 2.2 g/L sodium bicarbonate, 2% penicillin/streptomycin, 25mM HEPES, 5% FBS). Cells received fresh media 24 hours after plating.

Micropatterning

Polydimethylsiloxane (PDMS) stamps with 20μm wide rows spaced 3μm apart were used to print the micropattern onto 20mm diameter circular PDMS coverslips. The stamps were sterilized by sonicating in 70% ethanol, air-dried, and covered in a 1:40 dilution of 0.1% fibronectin from human plasma (Sigma-Aldrich) in PBS for 1 hour. The fibronectin solution was then aspirated and the stamps were dried with compressed nitrogen gas. PDMS coverslips were also sterilized by sonicating in 70% ethanol and carefully placed in 6-well cell culture plates. The plates were treated in a UV-ozone cleaner (Jelight Company) for 8 minutes prior to stamping. Stamps were inverted onto the PDMS coverslips and carefully removed. 1% Pluronic F-127® (Sigma Aldrich) was then added to the wells to make unstamped areas hydrophobic. Coverslips were washed with PBS 3 times and stored at 4°C until NRVM plating.

Adenovirus expressing FLAG-tagged WT and mutant MYBPC3 constructs

Mutant human MYBPC3 constructs containing an N-terminal FLAG epitope tag were created via site-directed mutagenesis using the QuikChange II XL Kit (Agilent) from wild type human MYBPC3 cDNA. The adenovirus was created using the ViralPower™ Adenoviral Gateway® Expression Kit (Invitrogen) using the pAd/CMV/V5-DEST Gateway® vector, and amplified in HEK293A cells. Further amplification and titration was done by the University of Michigan Vector Core.

Immunofluorescence of NRVMs

NRVMs were washed in PBS and fixed in 4% paraformaldehyde (Sigma-Aldrich) for 15 minutes at room temperature. The cells were then permeabilized in 0.2% Triton X-100 (Sigma-Aldrich) for 10 minutes and blocked in 5% goat serum in PBS for 30 minutes at room temperature. All antibodies were prepared in 5% goat serum in PBS. Cells were then incubated with primary antibodies for 1 hour at room temperature, washed three times with PBS for 5 minutes each, and then incubated with secondary antibodies for 30 minutes at room temperature protected from light. After three 5-minute washes with PBS, cells were incubated with 200ng/mL DAPI for 8 minutes at room temperature protected from light. Due to issues with cross-reactivity, cells stained for MYBPC3 and FLAG received sequential incubations of FLAG for 1.5 hours, then goat anti-rabbit IgG Alexa Fluor 488 for 30 minutes, then MYBPC3 for 1 hour, and then goat anti-mouse IgG Alexa Fluor 594 for 30 minutes, with three 5-minute washes with PBS between each step. Coverslips were then lifted from the culture plates and mounted face-up onto slides and topped with glass coverslips using ProLong Diamond. Slides cured overnight at room temperature protected from light. Antibody concentrations: MYBPC3, rabbit polyclonal 1:1000 (custom, Samantha Harris, University of Arizona); FLAG M2, mouse monoclonal 1:200 (Sigma-Aldrich); Hsc70, mouse monoclonal, 1:200 (Enzo Life Sciences ADI-SPA-815); AlexaFluor 488 phalloidin, 1:1000 (ThermoFisher Scientific); goat anti-mouse IgG Alexa Fluor 594, 1:500 (ThermoFisher Scientific); goat anti-rabbit IgG Alexa Fluor 488. 1:500 (ThermoFisher Scientific).

Western Blotting

Cell lysates were collected in 1X Laemmli buffer with Roche Protease Inhibitor. 5% β-mercaptoethanol was added to the samples, which were then boiled for 5 minutes at 95°C. Samples were then loaded onto 26-well precast Tris-HCl 4-20% gradient gels (BioRad) and then transferred to nitrocellulose membranes. The gels were stained in Biosafe Coomassie for 1 hour at room temperature and allowed to destain in ddH_2O overnight at 4°C. Nitrocellulose membranes were blocked in 5% non-fat dry milk in PBS for 1 hour at room temperature. All antibodies were prepared in 5% milk in 0.03% Tween-20 in PBS. Membranes were incubated with primary antibodies for 1 hour at room temperature or overnight at 4°C. Membranes were washed with 0.03% Tween-20 in PBS three times for 5 minutes each and then incubated with secondary

antibodies for 1 hour at room temperature protected from light. Blots and gels were scanned using an Odyssey® CLx Imaging System (LI-COR) and analyzed with LI-COR Image Studio™. Antibody Concentrations: MYBPC3, rabbit polyclonal 1:10000 (custom, provided by Samantha Harris, University of Arizona); FLAG M2, mouse monoclonal 1:1000 (Sigma-Aldrich F1804); FLAG, rabbit polyclonal 1:500 (Sigma-Aldrich F7425) Hsc70, mouse monoclonal 1:500 (Enzo Life Sciences ADI-SPA-815); Hsp70, mouse monoclonal 1:200 (Enzo Life Sciences ADI-SPA-810); α-actinin, mouse monoclonal 1:5000 (AbCam); cardiac myosin heavy chain (BA-G5), mouse monoclonal 1:1000 (AbCam), GAPDH, rabbit polyclonal 1:1000 (Millipore ABS16); IRDye® 680RD goat anti-mouse IgG 1:5000 (LI-COR); IRDye® 800CW goat anti-rabbit IgG 1:5000 (LI-COR).

Immunoprecipitation and mass spectrometric analysis of MYBPC3-interacting proteins

Unpatterned NRVMS were plated at a density of $1x10^7$ cells per 100mm culture dish. Cells were transduced with WT or truncated MYBPC3 adenovirus at MOI 10 24 hours after plating. Cells were collected 48 hours later by scraping in ice cold PBS with Roche protease inhibitor cocktail; cell pellets were stored at -80°C. $2x10^7$ cells were used per sample. Pellets were lysed in RIPA buffer (1% Triton X-100, 1% sodium deoxycholate, 0.1% SDS, 150mM NaCl, 10mM Na_2PO_4 pH 7.2, 1mM NaF, 1mM EDTA, 2.5mM EGTA, 20mM $(NH_4)_2MoO_4$, 100μM Na_3VO_4, Roche protease inhibitor cocktail) and incubated on ice for 15 minutes. Lysates were then sonicated for four 10 second bursts at 50% amplitude using a Branson digital sonifier with cup horn attachment, incubated on ice for a further 15 minutes, and centrifuged for 10 minutes at 13,000 rpm at 4°C to remove debris. Supernatants were recovered and protein concentration was determined by Bradford protein assay. This fraction was used as 'input' for Western blot analysis of co-IPs. 2mg of protein from supernatants was allocated to one FLAG co-IP tube and one negative control normal mouse IgG tube. All samples underwent initial pre-clearing of nonspecific interactors by adding 10μg of normal mouse IgG for one hour at 4°C followed by adding 20μL of a 1:1 mixture of protein A and protein G sepharose bead slurry (Sigma-Aldrich) for one hour at 4°C with gentle shaking. Pre-cleared supernatant was retained for IP. FLAG co-IP tubes received 20μL anti-FLAG M2-conjugated sepharose beads (Sigma-Aldrich) while negative control tubes received 10μg normal mouse IgG and 20μL 1:1 mix of protein A/protein G sepharose beads. Following overnight incubation at 4°C with gentle shaking, bead fractions were collected and immunoprecipitate was eluted by competitive binding in 100μL 100μg/mL 3X FLAG peptide (Sigma-Aldrich). Western blot analysis confirmed that FLAG-tagged MYPBC3 bait proteins were not non-specifically pulled down by normal mouse IgG negative controls. For mass spectrometry analysis, 30μL of the FLAG immunoprecipitate was separated by SDS-PAGE. Gels were stained in Biosafe Coomassie (BioRad) for 1 hour at room temperature and destained in ddH_2O for 1 hour. Gel lanes were cut into approximately 10 fragments according to molecular weight and tryptically digested. Mass spec data was acquired by nano-RP-LC-MS/MS analysis on an Orbitrap Tribrid Fusion instrument (ThermoFisher Scientific). Data was collected for two independent IP-MS experiments. Peptide-to-spectrum assignments (PSMs) were statistically validated using PeptideProphet.[39] The ABACUS algorithm was used to extract spectral counts, making adjustments for shared peptides among closely homologous proteins.[40] To identify MYBPC3 interacting proteins, only proteins detected in both experimental replicates with a calculated fold change in adjusted spectral counts of ≥2 over control samples in at least one replicate were considered. Spectral counts of interacting proteins were normalized to abundance of the FLAG-MYBPC3 bait protein. When comparing spectral counts for interacting proteins between WT and mutant MYBPC3, we verified that the majority of MYBPC3 peptides detected in each sample could be attributed to the human FLAG-MYBPC3 bait protein as opposed to any endogenous rat MYBPC3 that was pulled down non-specifically.

Cycloheximide pulse-chase assay

Unpatterned NRVMs were plated at a density of $2.5x10^5$ cells per well in 24-well culture plates and transduced at MOI 2 with wild type and mutant MYBPC3 adenovirus 24 hours after plating. After 48 hours, the cells received either: 20 μM scrambled siRNA (Silencer Select Negative Control #1, Thermofisher Scientific), 20 μM rat Hsc70 siRNA (Silencer Select s127902, ThermoFisher Scientific), 1:1000 DMSO vehicle, or 10 μM YM-1 (provided by Jason Gestwicki, UCSF) in DMSO. siRNA was incubated with Dharmafect 1 transfection reagent (DharmaCon) in antibiotic-free maintenance media (Media 199 with Earle's salts, L-glutamine, 2.2 g/L sodium bicarbonate, 25mM HEPES, 5% FBS) for 20 minutes before addition to the cells. 24 hours later, maintenance media (media used above with 2% penicillin/streptomycin) containing 300μg/mL cycloheximide (Sigma-Aldrich) was added to the cells. Cell lysates were collected by scraping the cells in 30μL of 1X Laemmli Buffer (BioRad) with Roche Protease Inhibitor cocktail at various time points from 0-12 hours post cycloheximide addition. Samples were snap-frozen in dry ice and stored at -80°C until western blot analysis was done to determine FLAG-tagged MYBPC3 WT, FLAG-tagged mutant MYBPC3, α-actinin, cardiac myosin heavy chain, and Hsc70 protein levels at the various time points. Data points were fitted to a first-order exponential decay curve ($y=e^{-kx}$) using GraphPad Prism software. Control and treatment decay curves were compared to determine if the results could be explained by the same reaction constant k.

MYBPC3 Protein Stability Analysis via AlphaLISA Experiment

Unpatterned NRVMs were plated at a density of $3.5x10^4$ cells per well in a 96 well plate. Cells were transduced with WT or truncated MYBPC3 adenovirus at MOI 2 or 10 24 hours after plating. Cycloheximide was added to various wells at different timepoints. After all timepoints were completed, the cells were washed with PBS and collected in 30 μL AlphaLISA Lysis Buffer (Perkin Elmer). The 96 well plates were placed on a plate shaker to life the cells. MYBPC3 N-terminus (Santa Cruz) antibody was conjugated to donor beads at a 1:1000 AB ratio concentration and 1:100 bead concentration in AlphaLISA immunoassay buffer (Perkin Elmer). Anti-FLAG conjugated to acceptor beads (Perkin Elmer) was prepared at 1:1000 concentration in AlphaLISA immunoassay buffer (Perkin Elmer). 5 μL of each cell lysate was added in duplicate to a white 96 well ½ AreaPlate (Perkin Elmer). 10 μL of the antibody-donor beads and 10 μL of the antibody-acceptor beads were added to each well. The plates were centrifuged at 1000 rpm for 1 minute and stored overnight at room temperature protected from light. The plates were read on an EnVision Multilabel plate reader at 615 nm wavelength. Values were normalized to the results from control NRVMs (no adenovirus transduction) and fitted to a first-order exponential decay curve ($y=e^{-kx}$) using GraphPad Prism software. Decay curves were compared to determine if the results could be explained by the same reaction constant k.

Hsc70 nuclear colocalization analysis

NRVMs were plated on micropatterned PDMS coverslips at a density of $1.5x10^5$ cells per well in a 6-well culture plate. The cells were immunostained for Hsc70 and phalloidin and the slides were imaged using a Nikon A1 confocal laser microscope system. 60X magnification Z-stack images with a step size of 0.6 μm were taken of 5-6 individual nuclei from three random fields per coverslip per condition. Colocalization analysis was done using NIS Elements Confocal imaging software.

Absolute Quantification of Abundance (AQUA)

Ventricular myocardial tissue from a patient with the Arg502Trp MYBPC3 mutation (Stanford Medical Center) was collected during a myectomy and non-failing ventricular myocardial tissue was collected from unmatched donor hearts from the University of Michigan. Myofilament proteins were separated using SDS-

PAGE using a 16-well precast Tris-HCl 4-20% gradient gels (BioRad) for four hours at 25 mA. The gel was then coomassie stained and MYBPC was excised. Gel bands were washed with 50mM Tris-HCl (pH 8.0) followed by acetonitrile. Samples were reduced with 10mM dithiothreitol at 60°C followed by alkylation with 50mM iodoacetamide at room temperature. Digestion with trypsin and chymotrypsin at 37°C for 18 hours using activation buffer (50mM Tris-HCl, 50mM DTT, 2mM EDTA). Supernatant was acidified with formic acid and analyzed directly without further processing. Samples were analyzed by nano LC/MS/MS with a Waters NanoAcquity HPLC system interfaced to a ThermoFisher Q Exactive. Peptides were loaded on a trapping column and eluted over a 75μm analytical column at 350nL/min; both columns were packed with Luna C18 resin (Phenomenex). The mass spectrometer was operated in data-dependent mode, with MS and MS/MS performed in the Orbitrap at 70,000 FWHM and 17,500 FWHM resolution, respectively. The fifteen most abundant ions were selected for MS/MS.

Procurement of Human Heart Tissue.

Acquisition of myocardial tissue from the intraventricular septum excised during surgical myectomy in HCM patients was described previously (50). Samples were collected with the approval of the University of Michigan Institutional Review Board, and all subjects gave informed consent.

Acknowledgements

I would like to thank my mentor, Dr. Sharlene Day, for giving me the opportunity to complete my thesis in her lab. I will be forever grateful for your unconditional support and guidance that has given me the confidence to develop my own ideas and design my own experiments. My experiences in your lab have informed my passion for medical research and my decision to further pursue it in my future. I will always consider you as one of my closest mentors and will always look up to you as a role model.

I would like to thank Amelia Glazier for teaching me how to be a better scientist. I greatly appreciate all the help and guidance you have given me in the lab these last few years. From your patience when I asked perhaps too many questions to our late-night scientific discussions that seemingly always turn into rants about politics, you have been instrumental in making this thesis possible.

I would also like to sincerely thank everyone else in the Day lab, who have made my experiences in the lab so enjoyable and memorable over the years. I would especially like to thank Jaime Yob for all her advice and support when I was conducting my experiments.

Lastly, I would like to thank my friends and family for their constant support in my life. I would especially like to thank my parents for always encouraging me to pursue my dreams and for being so understanding when I returned to campus early during holiday breaks or weekends to go into the lab.

References

1. Alcalai R, Seidman JG, Seidman CE. Genetic Basis of Hypertrophic Cardiomyopathy : From Bench to the Clinics. *J Cardiovasc Electrophysiol*. 2008;19:104-110.
2. Viswanathan SK, Sanders HK, Mcnamara JW, et al. Hypertrophic cardiomyopathy clinical phenotype is independent of gene mutation and mutation dosage. 2017:1-19.
3. Ueda Y, Stern JA. A One Health Approach to Hypertrophic Cardiomyopathy. *Yale J Biol Med*. 2017;90(3):433-448.
4. Alfares AA, Kelly MA, McDermott G, et al. Results of clinical genetic testing of 2,912 probands with hypertrophic cardiomyopathy: Expanded panels offer limited additional sensitivity. *Genet Med*. 2015;17(11):880-888.
5. Olivotto I, Maron MS, Adabag AS, et al. Gender-Related Differences in the Clinical Presentation and Outcome of Hypertrophic Cardiomyopathy. *J Am Coll Cardiol*. 2005;46(3):480-487.
6. Arad M, Seidman JG, Seidman CE. Phenotypic diversity in hypertrophic cardiomyopathy. *Hum Mol Genet*. 2002;11(20):2499-2506.
7. Maron BJ, Gardin JM, Flack JM, Gidding SS, Kurosaki TT, Bild DE. Prevalence of Hypertrophic Cardiomyopathy in a General Population of Young Adults. *Circulation*. 1995;92(4):785 LP-789.
8. Roma-rodrigues C, Fernandes AR. Genetics of hypertrophic cardiomyopathy : advances and pitfalls in molecular diagnosis and therapy. 2014:195-208.
9. Houston BA, Stevens GR. Clinical Medicine Insights : Cardiology. 2014;8:53-65.
10. Bos JM, Towbin JA, Ackerman MJ. Diagnostic, Prognostic, and Therapeutic Implications of Genetic Testing for Hypertrophic Cardiomyopathy. *J Am Coll Cardiol*. 2009;54(3):201-211.
11. McKenna WJ. Hypertrophic cardiomyopathy: management, risk stratification, and prevention of sudden death. *Heart*. 2002;87(2):169-176.
12. Christiaans I, Nannenberg EA, Dooijes D, et al. Founder mutations in hypertrophic cardiomyopathy patients in the Netherlands. 2010;18(5):248-254.
13. Flashman E, Watkins H, Redwood C. Localization of the binding site of the C-terminal domain of cardiac myosin-binding protein-C on the myosin rod. 2007;102:97-102.
14. Previs MJ, Previs SB, Gulick J, Robbins J, Warshaw DM. Molecular Mechanics of Cardiac Myosin-Binding Protein C in Native Thick Filaments. *Science (80-)*. 2012;337(6099):1215-1218.
15. Kuo PL, Lee H, Bray MA, et al. Myocyte shape regulates lateral registry of sarcomeres and contractility. *Am J Pathol*. 2012;181(6):2030-2037.
16. Bezold KL, Shaffer JF, Khosa JK, Hoye ER, Harris SP. A Gain-of-Function Mutation in the M-domain of Cardiac Myosin-binding Protein-C Increases Binding to Actin. 2013;288(30):21496-21505.
17. Gupta MK, Gulick J, James J, Osinska H, Lorenz JN, Robbins J. Functional dissection ofmyosin binding protein C phosphorylation. *J Mol Cell Cardiol*. 2013;64:39-50.
18. Keren A, Syrris P, McKenna WJ. Hypertrophic cardiomyopathy: the genetic determinants of

clinical disease expression. *Nat Clin Pract Cardiovasc Med*. 2008;5(3):158-168.

19. Saltzman AJ, Mancini-dinardo D, Li C, et al. Common Cause of Hypertrophic Cardiomyopathy. 2011;106(9):1549-1552.
20. Knöll R. Myosin binding protein C: Implications for signal-transduction. *J Muscle Res Cell Motil*. 2012;33(1):31-42.
21. Marian AJ. Hypertrophic cardiomyopathy: From genetics to treatment. *Eur J Clin Invest*. 2010;40(4):360-369.
22. Akerfelt M, Morimoto RI, Sistonen L. Heat shock factors: integrators of cell stress, development and lifespan. *Nat Rev Mol Cell Biol*. 2010;11(8):545-555.
23. Balch WE, Morimoto RI, Dillin A, Kelly JW. Adapting Proteostasis for Disease Intervention. *Science (80-)*. 2008;319(5865):916-919.
24. Morimoto RI. The Heat Shock Response : Systems Biology of Proteotoxic Stress in Aging and Disease. *Cold Spring Harb Symp Quant Biol*. 2012;LXXVI.
25. Fang X, Bogomolovas J, Wu T, et al. Loss-of-function mutations in co-chaperone BAG3 destabilize small HSPs and cause cardiomyopathy. *J Clin Invest*. 2017;127(8):3189-3200.
26. Colvin T, Gabai V, Gong J, et al. Hsp70-Bag3 interactions regulate cancer-related signaling networks. *Cancer Res*. 2014;74(17):4731-4740.
27. Yang Q, Sanbe A, Osinska H, Hewett TE, Klevitsky R, Robbins J. A mouse model of myosin binding protein C human familial hypertrophic cardiomyopathy. *J Clin Invest*. 1998;102(7):1292-300.
28. Foot NC. The Masson Trichrome Staining Methods in Routine Laboratory Use. *Stain Technol*. 1933;8(3):101-110.
29. Varnava A, Elliott P, Baboonian C, Davison F, Davies M, McKenna W. Hypertrophic cardiomyopathy. *Circulation*. 2001;104:1380-1384.
30. Feng H-Z, Jin J-P. A protocol to study ex vivo mouse working heart at human-like heart rate. *J Mol Cell Cardiol*. 2017;114(October 2017):175-184.
31. Moore BB, Hogaboam CM. Murine models of pulmonary fibrosis. *Am J Physiol - Lung Cell Mol Physiol*. 2008;294(2):L152 LP-L160.
32. Helms AS, Davis F, Coleman D, et al. Sarcomere Mutation-Specific Expression Patterns in Human Hypertrophic Cardiomyopathy. *Circ Cardiovasc Genet*. 2014;7(4):434-443.
33. McDonough H, Patterson C. CHIP: a link between the chaperone and proteasome systems. *Cell Stress Chaperones*. 2003;8(4):303-308.
34. Wang AM, Miyata Y, Klinedinst S, et al. Activation of Hsp70 reduces neurotoxicity by promoting polyglutamine protein degradation. *Nat Chem Biol*. 2013;9(2):112-118.
35. Buchberger A, Theyssen H, Schroder H, et al. Nucleotide-induced conformational changes in the ATPase and substrate binding domains of the DnaK chaperone provide evidence for interdomain communication. *J Biol Chem*. 1995;270(28):16903-16910.
36. Knowlton AA, Salfity M. Nuclear localization and the heat shock proteins. *J Biosci*. 1996;21(2):123-132.

37. Li Y, Zhang T, Zhang X, Wang G, Wang Y, Zhang Z. Heat shock cognate 70 gene in Haliotis diversicolor: responses to pathogen infection and environmental stresses and its transcriptional regulation analysis. *Cell Stress Chaperones*. 2017.

38. Rahman KMZ, Mamada H, Takagi M, Kose S, Imamoto N. Hikeshi modulates the proteotoxic stress response in human cells: Implication for the importance of the nuclear function of HSP70s. *Genes to Cells*. 2017;(August):968-976.

39. Ma K, Vitek O, Nesvizhskii AI. A statistical model-building perspective to identification of MS/MS spectra with PeptideProphet. *BMC Bioinformatics*. 2012;13(Suppl 16):S1.

40. Fermin D, Basrur V, Yocum AK, Nesvizhskii AI. Abacus: A computational tool for extracting and pre-processing spectral count data for label-free quantitative proteomic analysis. *Proteomics*. 2011;11(7):1340-1345.